

1 **APOBEC2 is a Transcriptional Repressor required for proper Myoblast Differentiation**

2
3 Jose Paulo Lorenzo^{1a}, Linda Molla^{2a}, Ignacio L. Ibarra^{3,4}, Sandra Ruf¹, Jana Ridani^{5,6},
4 Poorani Ganesh Subramani^{5,6}, Jonathan Boulais⁵, Dewi Harjanto², Alin Vonica⁷, Javier M. Di
5 Noia^{5,6,8}, Christoph Dieterich⁹, Judith B. Zaugg³, F. Nina Papavasiliou^{*1,2}

6 7 **Affiliations:**

8 ¹ Division of Immune Diversity, German Cancer Research Center (DKFZ), 69120
9 Heidelberg, Germany

10 Faculty of Biosciences, Heidelberg University, 69117 Heidelberg, Germany

11 ² Laboratory of Lymphocyte Biology, The Rockefeller University, New York, NY 10065, USA

12 ³ Structural and Computational Biology Unit, European Molecular Biology Laboratory,
13 Heidelberg, Germany

14 ⁴ Institute of Computational Biology, Helmholtz Zentrum München, German Research Center
15 for Environmental Health, Neuherberg, Germany

16 ⁵ Institut de Recherches Cliniques de Montréal, 110 av. des Pins Ouest, Montréal, QC,
17 Canada H2W 1R7

18 ⁶ Department of Medicine, Division of Experimental Medicine, McGill University, 1001 boul
19 Decarie, Montréal, QC, Canada H4A 3J1

20 ⁷ Department of Biology, The Nazareth College, Rochester, NY 14618, USA

21 ⁸ Department of Medicine, Université de Montréal, C.P. 6128, succ. Centre-ville, Montréal,
22 QC, Canada, H3C 3J7

23 ⁹ Klaus Tschira Institute for Integrative Computational Cardiology, University Hospital
24 Heidelberg, Heidelberg, Germany

25
26 ^aThese authors contributed equally to the work

27 *Corresponding Author: F. Nina Papavasiliou (n.papavasiliou@dkfz-heidelberg.de)

28 29 30 31 **ABSTRACT**

32
33
34 The activation induced cytidine deaminase/apolipoprotein B editing complex (AID/APOBEC)
35 family comprises several nucleic acid editors with roles ranging from antibody diversification
36 to mRNA editing. APOBEC2, an evolutionarily conserved member of this family, has neither
37 an established substrate nor a mechanism of action, however genetic evidence suggests
38 functional relevance in tissues such as muscle. Here, we demonstrate that in muscle,
39 APOBEC2 does not have any of the attributed molecular functions of the AID/APOBEC
40 family, such as RNA editing, DNA demethylation, or DNA mutation. Instead, we show that
41 APOBEC2 occupies chromatin at promoter regions of certain genes, whose expression is
42 repressed during muscle cell differentiation. We further demonstrate that APOBEC2 on one
43 hand binds promoter region DNA directly and in a sequence specific fashion, while on the
44 other it interacts with HDAC transcriptional corepressor complexes. Therefore, APOBEC2,
45 by actively repressing the expression of non-myogenesis pathway genes, plays a key role in
46 enforcing the proper establishment of muscle cell fate.

47
48

49 The AID/APOBEC proteins are zinc-dependent deaminases that catalyze the
50 removal of the amino group from a cytidine base in the context of a polynucleotide chain,
51 resulting in cytidine (C) to uridine (U) transition on DNA or RNA. Members of the
52 AID/APOBEC family are closely related to one another based on homology and conservation
53 of the cytidine deaminase domain containing a zinc-dependent deaminase sequence motif ¹.
54 However, they differ by tissue-specific expression, substrates, and biological functions
55 (reviewed in ²). Physiologically these proteins alter the informational content encoded in the
56 genome through a range of processes: acting as messenger RNA (mRNA) editors, affecting
57 translation (APOBEC1) ^{3,4}, acting as DNA mutators to create novel gene variants, restrict
58 viruses and retrotransposons (AID and APOBEC3) (reviewed in ⁵) and, changing DNA 5mC
59 modification levels, leading to modulation of transcript abundance (AID and APOBEC1) ^{6,7}.

60
61 APOBEC2 is an evolutionarily conserved member of the AID/APOBEC family ⁸.
62 Substantial evidence highlights the biological relevance of APOBEC2 in metazoans. In mice,
63 APOBEC2 is highly expressed in cardiac and skeletal muscle where it affects muscle
64 development ⁹. Specifically, in the absence of APOBEC2, there is a shift from fast to slow
65 muscle fiber formation, a reduction in muscle mass, and a mild myopathy with age ¹⁰. In
66 zebrafish, APOBEC2 has been implicated in muscle fiber arrangement ¹¹ and in retina and
67 optic axon regeneration ¹². In frogs, APOBEC2 is important in left-right axis specification
68 during early embryogenesis ¹³. Mutations and gene expression changes of APOBEC2 have
69 also been linked to cancer development ^{14,15}.

70
71 Even though there is evidence for a biological role of APOBEC2, there are few
72 insights to the mechanism by which APOBEC2 accomplishes these. Moreover, there has
73 been no definite demonstration of its activity as a cytidine deaminase. Based on its
74 homology with the other AID/APOBEC family members, it has been hypothesized that
75 APOBEC2 may be involved in RNA editing ^{9,14} or DNA demethylation ^{6,7,12}. It has also been
76 hypothesized that it has lost its deaminase activity altogether and may act biologically by a
77 different mechanism ¹⁶. However, there is currently a lack of knowledge on the direct
78 physiological targets of APOBEC2, and its mechanism of action.

79
80 To answer some of these questions, we performed knockdown studies of APOBEC2
81 during the differentiation of the C2C12 murine myoblast cell line to systematically
82 characterize the transcriptome and DNA methylation patterns of APOBEC2 deficient C2C12
83 cells. Our results confirm the requirement of APOBEC2 for myoblast to myotube
84 differentiation. Additionally, we demonstrate the requirement of its amino-terminal disordered
85 region for nuclear localization and myotube differentiation. While our results do not support

86 APOBEC2 roles on RNA editing and on DNA methylation, we find that APOBEC2
87 downregulation leads to substantial gene expression changes affecting programs associated
88 with myogenesis. Moreover, genomic occupancy experiments demonstrate that APOBEC2
89 interacts with chromatin at promoters of genes that are repressed during myoblast
90 differentiation. Furthermore, these targets are derepressed with reduced abundance of
91 APOBEC2, which allude to APOBEC2 acting as a transcriptional repressor. Notably, these
92 target derepressed genes are not directly involved in myogenesis or muscle differentiation;
93 instead they seem enriched for genes in the innate immune / inflammatory pathway. Finally,
94 we show that APOBEC2 directly interacts with DNA as well as Histone Deacetylase 1
95 (HDAC1) repressor complexes, which supports the molecular function of APOBEC2 as a
96 transcriptional repressor. Taken together, our data suggest that APOBEC2 has a direct role
97 in regulating active gene transcription during myoblast differentiation as a transcriptional
98 repressor.

99

100 ***APOBEC2 is required for myoblast to myotube differentiation***

101

102 The C2C12 myoblast cell line was derived from mouse satellite cells activated to
103 proliferate after muscle injury in adult mice ¹⁷. C2C12 myoblasts are thought to recapitulate
104 the first steps of muscle differentiation in culture and upon differentiation induce APOBEC2
105 expression ¹³ (Supplementary Fig. 1A), making them a suitable model to investigate putative
106 roles of this suspected cytidine deaminase in situ.

107

108 To explore the role of APOBEC2 during myogenesis, we reduced APOBEC2 protein
109 levels with short hairpin RNA (shRNA) against APOBEC2 mRNA. Protein reduction was
110 efficient and coincided with reduced myoblast-to-myotube differentiation, evidenced by the
111 decrease in expression of TroponinT and myosin heavy chain (MyHC), protein markers of
112 late differentiation (Fig. 1A). At the cellular level downregulation of APOBEC2 protein levels
113 coincided with reduced myotube formation (Fig. 1B). These observations match those
114 previously reported using mouse embryonic stem cell-derived myogenic precursors ¹⁸.

115

116 We then restored APOBEC2 protein in these knockdown cells through
117 overexpression. This led to an increase in MyHC levels, which confirms the essential role of
118 APOBEC2 in myoblast differentiation in this model (Fig.1C). Additionally, we produced
119 truncated APOBEC2 (residues 41-224 mouse APOBEC2) based on its published structures
120 ^{19,20}. Truncated APOBEC2 (del(2-40)A2), was unable to restore MyHC expression levels.
121 Interestingly, the truncated form of APOBEC2 was only found in the cytoplasmic fraction of
122 differentiated C2C12 myoblasts (Supplementary Fig. 1C). We speculated that the nuclear

123 localization of APOBEC2 was necessary for its role in muscle differentiation and pointed to a
124 molecular function within the nuclear compartment.

125

126 ***APOBEC2 loss leads to gene expression changes related to muscle differentiation***

127

128 To study how APOBEC2 loss leads to problems in C2C12 myoblast-to-myotube
129 differentiation, we performed RNA sequencing (RNA-Seq) to compare the transcriptome
130 dynamics of APOBEC2 knockdown and control cells during differentiation. We observed that
131 reduced APOBEC2 levels led to substantial gene expression changes (Fig. 1D,E). Notably,
132 genes downregulated during differentiation were enriched for muscle development Gene
133 Ontology (GO) terms, whereas genes upregulated were enriched for GO terms related to
134 immune response (Fig. 1C; Supplementary File 1). The decreased expression of muscle
135 differentiation related genes reflects the observed reduced myotube formation. Though
136 undetectable on the immunoblot (Fig. 1A), perturbation of APOBEC2 levels prior to inducing
137 differentiation seems to affect the potential of C2C12 to differentiate into myotubes. Genes
138 involved in muscle development or function were also downregulated at day 0 prior to
139 inducing the cells to differentiate.

140

141 Furthermore, genes related to cell development or differentiation GO terms,
142 particularly immune system development, blood vessel development, and nervous system
143 development, are among those overrepresented in the list of upregulated genes with
144 APOBEC2 deficiency (Supplementary File 2). These spurious non-muscle transcriptional
145 programs possibly reflect transdifferentiation events, which have been observed for C2C12
146 myoblasts ²¹.

147

148 We next investigated possible molecular mechanisms of how APOBEC2 causes
149 these gene expression changes. Due to the conserved cytidine deaminase domain within
150 the AID/APOBEC family, APOBEC2 is posited to be an RNA editor ^{9,14} and a DNA
151 demethylase ^{6,7,12}. Upon comparing the transcriptomes of the APOBEC2 knockdown and
152 control C2C12 cells for instances of C-to-U RNA editing, using a previously validated
153 pipeline ²², we could not identify C-to-U or A-to-I RNA editing events that were APOBEC2
154 dependent (Supplementary Fig. 2A). Similarly, using bisulfite sequencing, we were unable to
155 observe significant methylation differences between the APOBEC2 knockdown and control
156 C2C12 cells that could account for the gene expression changes (Supplementary Fig. S2B-
157 C). Altogether, these results strongly indicate that APOBEC2 is neither involved in mRNA
158 deamination nor DNA demethylation in differentiating muscle.

159

160

161 ***APOBEC2 binds promoter regions***

162

163

164 Cytidine deaminases of the AID/APOBEC family can bind and mutate DNA either at
165 gene bodies, e.g. exons of the immunoglobulin locus, as catalyzed by AID, reviewed in ²³ or
166 at promoter regions, e.g. local hypermutations as catalyzed by APOBEC3 family members -
167 reviewed in ²⁴. To assess whether APOBEC2 could also bind genomic DNA, we first
168 determined the subcellular localization of APOBEC2 in muscle cells. We observe that
169 APOBEC2 is present in both the cytoplasm and nucleus of differentiated C2C12 myotubes
170 (Fig. 2A, Supplementary Fig. 1C). A weak nuclear localization signal (NLS) can be predicted
171 by cNLS Mapper ²⁵ (APOBEC2 residues 26 to 57, with a score of 3.7) that could explain the
172 lack of nuclear localization of truncated APOBEC2, del(2-40)A2. However, full length
173 APOBEC2 does not show NLS activity but is homogenously distributed throughout the cell,
174 presumably through passive diffusion ²⁶. To then assess whether nuclear APOBEC2 could
175 bind chromatin, we utilized sequential salt extraction based on the principle that loosely
176 bound proteins will be dissociated at low salt concentration, while tightly bound ones will not
177 ²⁷. Using this technique, we found that a fraction of APOBEC2 within differentiating C2C12
178 cells, remains bound to chromatin even at high salt concentrations (up to 1 M NaCl). As a
179 comparison histone H4 dissociates completely from DNA at 0.75 M NaCl (Fig. 2B). These
180 data suggest a strong association of nuclear APOBEC2 with chromatin in differentiating
181 myoblasts.

181

182 To determine APOBEC2 binding localization within chromatin, we performed
183 chromatin immunoprecipitation-sequencing (ChIP-Seq) experiments, and calculated
184 enrichment of APOBEC2 at specific loci over input using MACS2 (see Methods). We
185 performed each experiment in triplicate, and only peaks that were called in at least 2 out of 3
186 replicates were analyzed. Importantly, we queried APOBEC2 occupancy at two different time
187 points, 14- and 34-hours post-differentiation, that precede the RNA-Seq time points, where
188 we observed changes in gene expression and represent time points of low and higher
189 APOBEC2 protein abundance. Overall, the signal around peak summits of transcription start
190 sites (TSS) is higher at 34 versus 14 hours, reflecting an increase of APOBEC2 in
191 chromatin. In contrast, input controls show lower enrichment over the peak summits (Fig.
192 2C).

193

194 Annotating the APOBEC2 peaks by genomic feature showed that for both time points
195 most of the peaks fall within promoters, defined as regions -2 kilobases (kb) to +2 kb around
196 the TSS (Fig. 2D). Next, we wanted to determine whether APOBEC2 occupies specific
197 motifs within promoter regions. The members of the AID/APOBEC family that bind to DNA

198 have some local sequence preference with regard to sites they mutate, but do not display
199 rigorous sequence specificity, e.g. akin to transcription factor (TF) binding sites²⁸. To assess
200 the motif signatures in those regions we queried through motif enrichment the over-
201 representation of TF 8-mers sequences associated to main TF modules²⁹. Among 108 TF
202 modules tested against a controlled background of negative sequences (see Methods), we
203 observed 19 of those significantly enriched at APOBEC2 regions in at least one
204 differentiation time point. SP and KLF motifs were among the top enrichments observed (Fig.
205 2E), suggesting a co-regulatory role between these factors and APOBEC2. In general, TF
206 specificity groups increase their significance between 14 and 34 hours but with lower overall
207 effect sizes or only at the later time points, suggesting that the interplay between TFs and
208 APOBEC2 occupied regions is specific at 14 hours but broader at later time points, likely as
209 consequence of events related to its early binding. Additionally, we did not observe
210 APOBEC2 related DNA mutation at the occupied peaks, indicating that APOBEC2 is not a
211 DNA mutator like other AID/APOBEC family members (Supplementary Fig. 3).

212 ***APOBEC2 represses expression of occupied genes***

213
214 Focusing on the promoter bound genes we determined that there are ~1500 genes
215 that are bound by APOBEC2 near their transcription start sites in any of the time points, 590
216 of which are occupied at both time points (Fig. 3A). Overall, about 79% of the genes that are
217 bound by APOBEC2 in the 14-hour time point remain bound at the 34-hour time point.
218 Further, using Gene Set Enrichment Analysis to determine the distribution of APOBEC2
219 occupied genes at both time points in a list of ranked expression changes either through
220 differentiation (day 0 to 2) or upon APOBEC2 knockdown (A2 shRNA vs GFP shRNA at day
221 2). Our results show that APOBEC2 occupied genes are significantly enriched at genes
222 downregulated through differentiation (Fig. 3B). Moreover, upon APOBEC2 knockdown,
223 APOBEC2 occupied genes are instead enriched at upregulated genes (Fig. 3C).
224 Interestingly, overall expression of APOBEC2 bound genes through C2C12 differentiation
225 from day 0 to 2 is significantly decreased during differentiation compared to genome wide
226 expression changes (-0.3 versus 0.1 mean log₂ fold changes; $t = -8.2$; adjusted P-values <
227 0.0001; Fig. 3D). Furthermore, expression of APOBEC2 occupied genes increase upon
228 APOBEC2 knockdown (t -statistic = 4.0; adjusted P-value < 0.001) highlighting a global
229 repressive role of APOBEC2 during differentiation. Altogether, these results suggest that the
230 observed transcriptional changes linked to APOBEC2 deficiency are due to APOBEC2
231 functioning as a transcriptional repressor.
232

233
234 To validate its possible role as a transcriptional repressor, we selected candidate
235 genes repressed by APOBEC2 occupancy. We narrowed it down to a list of genes occupied

236 by APOBEC2 which are downregulated during differentiation (day 2) and upregulated with
237 APOBEC2 knockdown. In this gene list, we did not find an overrepresentation of GO terms
238 relating to muscle differentiation; but rather, we found terms related to development of other
239 lineages (Supplementary Table S1) similar to the non-muscle genes upregulated with
240 APOBEC2 deficiency. Furthermore, a list of 31 genes related to differentiation (GO: 0045595
241 regulation of differentiation) in other tissue contexts were upregulated with APOBEC2 loss
242 (Fig. 3E). We speculate that APOBEC2 is acting as a repressor to direct C2C12
243 differentiation into the muscle-lineage by repressing specious gene networks related to other
244 lineages.

245 246 ***APOBEC2 binds directly to single- and double-stranded DNA*** 247

248 Thus far, the results suggest that APOBEC2 has a molecular role unique to the
249 AID/APOBEC family. While it does not have the capacity to modify nucleic acids (RNA or
250 DNA) through deamination^{30,31}, it is capable of binding chromatin to regulate transcription.
251 This implies either that APOBEC2 interacts directly with DNA at promoter regions, or that it
252 interacts with transcription regulators that do so, or both.

253
254 To assess whether APOBEC2 is capable of binding DNA directly, we generated
255 recombinant APOBEC2 (expressed in insect cells, Supplementary Fig. 4A) and tested it in
256 vitro for its capacity to bind DNA oligonucleotides that represent APOBEC2 bound
257 sequences in vivo. We tested an SP/KLF DNA motif as it was highly represented in the
258 ChIP-Seq data (Figure 4A). As a negative control, we tested an A-tract motif that based on
259 the ChIP-Seq was not bound by APOBEC2 but which occurred frequently at promoters of
260 differentially regulated genes. Using microscale thermophoresis (MST), purified APOBEC2
261 bound both single-stranded and double-stranded DNA containing the SP/KLF motif with
262 reasonable affinity (calculated $K_d = 253 \pm 86$ nM and 709 ± 186 nM, respectively, Figure 4A,
263 S4B). In contrast, measurements for the A-tract motif showed large variances between trials,
264 indicating lack of specific binding (Figure S4C). This ability to selectively bind both ssDNA
265 and dsDNA in a sequence-specific manner in vitro (Fig. 4A) and in vivo (Fig. 2E) makes
266 APOBEC2 unique among AID/APOBEC family members. These results demonstrate that
267 APOBEC2 can target specific genes at promoter regions, and through this binding repress
268 transcription.

269
270 Using gel electromobility shift assays (EMSA), we checked for APOBEC2
271 cooperativity with the transcription factor SP1 on its cognate motif. As expected, purified SP1
272 protein alone shifted dsDNA with the SP/KLF motif (lane 7, Fig. 4B). Unexpectedly, we were
273 unable to see a shift by APOBEC2 alone on either ssDNA or dsDNA unlike with MST (lanes

274 3 and 6, Fig. 4B). This could be due to the running conditions which were unable to preserve
275 the presumably weaker intermolecular affinity. However, APOBEC2 together with SP1
276 produced a shift with stronger intensity indicating cooperativity between the two DNA binding
277 proteins (lane 7 vs lane 8, Fig. 4B). Interestingly, the two do not interact directly
278 (Supplementary Fig. 4D), suggesting that the enhanced SP1 binding is mediated through
279 DNA – possibly through changes in DNA conformation given that APOBEC2 has no
280 detectable deaminase activity. This cooperativity suggests a molecular mechanism wherein
281 APOBEC2 alters transcription factor affinity for specific motifs leading to transcriptional
282 repression.

283 ***APOBEC2 interacts with corepressor complexes in vivo***

284
285 To ascertain the mechanism of action for the observed transcriptional repression, we
286 used proximity-dependent protein biotinylation (BioID) to confirm and identify other putative
287 APOBEC2 proximal protein complexes that may indicate direct interactions. After statistical
288 curation we identified 124 proteins that were significantly more tagged by APOBEC2-BirA
289 and/or BirA-APOBEC2 than GFP-BirA controls in C2C12 cells (Supplementary Table S2).
290 Functional annotation showed that many APOBEC2 neighboring proteins are related to cell
291 membrane and cytoskeleton organization processes, in line with its high cytoplasmic
292 abundance (Fig. 2B), but terms related to chromatin modification and histone deacetylation
293 were also enriched (Supplementary Fig. 5A and Supplementary Table S3). Of special
294 interest was the identification the histone deacetylase 1 (HDAC1) and Chromodomain-
295 helicase-DNA-binding protein 4 (CHD4), both components of the nucleosome remodeling
296 and histone deacetylation (NuRD) transcriptional corepressor complex ³², (Fig. 4C and
297 Supplementary Fig. 5B). Using co-IP, we validated that APOBEC2 interacts with HDAC1 in
298 differentiated C2C12 myoblasts (Fig. 4D). Together with the observation that APOBEC2
299 interacts directly with chromatin, this suggests that APOBEC2 plays a role in gene regulation
300 through epigenetic nucleosome modification with these transcriptional corepressor
301 complexes.
302

303
304 Taken together, our results suggest a direct role of APOBEC2 in repressing specific
305 transcribed genes, likely mediated by an HDAC1 co-repressor complex during C2C12
306 myoblast differentiation (Fig. 4F).

307 **DISCUSSION**

308
309 There have been many hypothesized roles for the cytidine deaminase APOBEC2.
310 Here we show that the expression of APOBEC2 during myoblast differentiation has
311 consequential effects on myotube formation owing to at least one unexpected molecular
312

313 function: transcriptional control. We discovered that APOBEC2 loss, leads to faulty myoblast
314 differentiation and concomitant gene expression changes. We show that these gene
315 expression changes come about through direct chromatin interaction of APOBEC2 at
316 promoters – with no observed APOBEC2 related changes in RNA editing, DNA methylation,
317 or DNA mutation. We find instead that APOBEC2 is capable of directly binding DNA and
318 interacting with corepressor complexes. Indeed, through this interaction, APOBEC2
319 specifically represses transcriptional programs unrelated to muscle differentiation thus
320 indirectly supporting proper muscle differentiation.

321

322 The deaminase domain of APOBEC2 appears to have lost catalytic activity ^{30,31}.
323 However, it seems to have retained its ability to bind nucleic acids. Binding ssDNA is nothing
324 new to members of the AID/APOBEC family ³³. However, the demonstration that APOBEC2
325 directly binds to dsDNA is groundbreaking for the family. There has been evidence for
326 APOBEC3-driven dsDNA mutation but no evidence for direct dsDNA binding; instead, the
327 mutational mechanism is likely through ssDNA ^{34,35}. Prior work has linked APOBEC2
328 overexpression to RNA editing of specific transcripts as observed in the healthy livers of
329 transgenic mice which eventually develop hepatocellular carcinoma ¹⁴. Notably, RNA editing
330 was only detectable in the liver at specific transcripts for the transgenic mice. However,
331 based on our transcriptome analysis, we were unable to find evidence of such RNA editing
332 in our myoblast differentiation models. Prior work has also reported mild effects of
333 APOBEC2 on DNA methylation specifically at the MYOG promoter ¹⁸; yet from our ChIP-Seq
334 data, we do not find occupancy at the MYOG gene. Furthermore, there is conflicting data on
335 the role of the AID/APOBEC family in active DNA demethylation; and, APOBEC2 dependent
336 demethylation has not been found in other cellular contexts ^{36,37}. A role in transcriptional
337 repression such as we propose, would also explain these prior data, as indirect effects of
338 improper differentiation.

339

340 Previous studies suggested that recombinant APOBEC2 is incapable of binding DNA
341 or deaminating it ^{16,30,31}. Our experiments using recombinant protein produced in eukaryotic
342 cells show that APOBEC2 is capable of binding DNA with reasonable affinity, and when it
343 does so, it alters the ability of proximal transcription factors (such as SP1) to interact with
344 their cognate motifs. Similar findings have also been observed with the transcription factor
345 POU6F2, suggesting but not proving a role for APOBEC2 in transcription ¹⁶.

346

347 Furthermore, our proximity ligation experiments reveal that APOBEC2 protein directly
348 interacts with HDAC1 and CHD4 containing repressor complexes providing a direct
349 epigenetic mechanism for the repression of APOBEC2 occupied genes. HDAC1 and CHD4

350 are components of the NuRD corepressor complex, whose involvement has already been
351 proposed in skeletal or myocardial muscle fate determination³⁸. Additionally, the abundance
352 of APOBEC2 in the cytoplasm and its proximity to proteins that participate in cell morphology
353 and the cytoskeleton could either reflect a mechanism limiting APOBEC2 access to the
354 nucleus, or perhaps an additional function that remains to be studied.

355

356 Uniquely amongst AID/APOBEC family members, the amino-terminus of APOBEC2
357 contains a region that is glutamate-rich and intrinsically disordered²⁰. Loss of this
358 unstructured domain results in inability of the protein to rescue the knockdown phenotype
359 likely through the loss of its nuclear retention. Proteins with similar disordered regions have
360 been shown to form liquid phase separated membrane-less compartments and this function
361 appears to be especially important for transcriptional regulation as transcription factors with
362 disordered regions have been shown to form such compartments³⁹. Even though, no
363 enzymatic activity has been detected for APOBEC2, potential substrates could be present in
364 these chromatin compartments: transient RNA species, eluding detection limits by our RNA-
365 Seq method, or, potentially, ssDNA structures at melted promoters. We propose that through
366 its N-terminal unstructured region APOBEC2 is retained in the nucleus where on one hand it
367 binds DNA at promoter regions in a sequence specific fashion, and on the other, it recruits
368 corepressor complexes to repress transcription.

369

370 We hypothesize that APOBEC2 acts as a modulator of its bound promoters during
371 the myogenic program – fine-tuning it for muscle differentiation and repressing other lineage
372 programs. MYOD1 has been shown to bind and activate lineage programs outside the
373 muscle lineage; however, this is mitigated by corepressors⁴⁰. Furthermore, as APOBEC2
374 expression under healthy conditions is mostly confined to muscle tissue (both skeletal and
375 heart), where it might be acting as a ‘many-but-muscle’ lineage repressor – similar to MYT1L
376 in neuronal differentiation⁴¹.

377

378 The discovery that APOBEC2 has a direct role in transcriptional control impacts how
379 we interpret the phenotypes that have been attributed to it in the mouse knockout models
380 and other biological systems, well beyond muscle differentiation – for example zebrafish
381 retina and optic nerve regeneration, *Xenopus* embryo development, and cancer
382 development^{12–14}. In the zebrafish models, APOBEC2 loss leads to similar defective muscle
383 phenotypes but it is deemed essential in the retinal regeneration model – where cellular
384 reprogramming is a key step¹². Directly or indirectly, these prior observations likely relate to
385 aberrant transcriptional programs, normally silenced in the context of tissue development or
386 cell differentiation due to APOBEC2 transcriptional control. Taken together, we postulate that

387 APOBEC2 is a transcriptional repressor that modulates transcriptional programs during cell
388 differentiation or reprogramming.

389 **Methods**

391 *Data availability*

392 High throughput sequencing datasets are all found in: GSE117732 and more specifically:
393 RNA-Seq (GSE117730); ChIP-Seq (GSE117729); ERRBS (GSE117731). Mass
394 spectrometry data for BioID performed in Flp-In 293 T-REx cells have been deposited in
395 MassIVE under ID.

398 *C2C12 cell culture*

399 C2C12 cells (CRL-1772, ATCC) were maintained in DMEM (30-2002, ATCC) with 10% fetal
400 bovine serum and fed every two days. To differentiate equal number of cells (2.5×10^5)
401 were seeded in 6-well plates followed by media change to DMEM with 2% horse serum after
402 12 hours. For generating single cell clones for RNA-Seq and RRBS experiments C2C12s
403 were sorted using fluorescence-activated cell sorting (FACS) and seeded into a 96 well
404 plate. Each clone was expanded and tested for successful knockdown through
405 immunoblotting.

408 *APOBEC2 knockdown and overexpression*

409 C2C12 cells were infected with lentiviruses carrying shRNA, targeting either APOBEC2 or
410 GFP. All APOBEC2 shRNAs were obtained from The Broad Institute's Mission TRC-1
411 mouse library and present in pLKO.1-puro construct. Plasmids used: pLKO.1 - TRC cloning
412 vector (Addgene, # 10878)⁴²; pLKO.1 puro GFP siRNA (Addgene, # 12273)⁴³. The design
413 of shRNAs and cloning in pLKO.1-TRC, were done according to the Addgene protocol
414 (Protocol Version 1.0. December 2006). The following shRNAs sequences were used for
415 APOBEC2 knockdown: A2 shRNA: GCTACCAGTCAACTTCTTCAA; GFP shRNA:
416 GCAAGCTGACCCTGAAGTTCAT.

417 Virions were produced by co-transfection of pLKO.1-puro shRNA containing construct,
418 packaging plasmid psPAX2 (Addgene, #12260) and envelope plasmid pMD2.g (Addgene,
419 #12259) in 293T cells (CRL-3216, ATCC). Transfections were done using Lipofectamine
420 2000 Reagent (Invitrogen) as per manufacturer instructions. Supernatants with lentiviral
421 particles were collected at 24 and 48 hours after transfection, passed through a 0.45 mm
422 filter and applied to C2C12s. For APOBEC2 constitutive knockdown, C2C12 cells were
423 infected with pLKO.1 containing lentiviruses in growth media containing 8 $\mu\text{g}/\text{mL}$ polybrene
424 for 12 hours. Two days after lentiviral infection cells were cultured with 4 $\mu\text{g}/\text{ml}$ puromycin
425 containing media for two more days to select cells stably expressing the shRNA.

426 Rescue constructs, mouse APOBEC2 and del(1-41)APOBEC2 with silent mutations to
427 escape shRNA knockdown, and tagged constructs, APOBEC2 and del(1-41)APOBEC2 with
428 C-terminal 3xHA-tags, were cloned into pMXs-GFP/Puro retroviral vectors (Cell Biolabs,
429 Inc.). Virions were produced in 293T cells by co-transfection with pMXs construct and pCL-
430 Eco (Novus Biologicals) using Lipofectamine 2000.

436 *Immunoblotting and co-immunoprecipitation*

437 For immunoblotting experiments, C2C12 cells were first washed with cold PBS and lysed in
438 100 μl RIPA lysis buffer (Santa Cruz, sc-24948) in 6-well plates. They were incubated at 4°C
439

441 for 15 minutes and then extracts were scrapped into a microfuge tube. Lysates were snap
442 frozen in liquid nitrogen. After thawing the lysates on ice and clearing out cell debris by
443 centrifugation, equal amounts of total protein (ranges between 10-30 μg) were boiled in
444 SDS-PAGE sample buffer and loaded onto each lane of a polyacrylamide gel (Criterion XT
445 Bis-Tris Gel 12%, Bio-Rad). Following electrophoresis, the resolved protein was transferred
446 to a nitrocellulose membrane and subjected to western blot analysis. The source and dilution
447 for each antibody used were: polyclonal rabbit-APOBEC2 (gift from Alin Vonica MD, PhD),
448 1:1000; monoclonal mouse-APOBEC2 (clone 15E11, homemade), 1:5000; TroponinT clone
449 JLT- 12 (T6277, Sigma-Aldrich), 1:500; alpha-tubulin DM1A (Abcam, ab7291), 1:5000;
450 MyHC MF-20 (DSHB), 1:20; rabbit anti-SP1 (Merck, 07-645), 1:1000; and rabbit anti-HDAC1
451 antibody (ab7028), 1:2000.

452
453 For co-immunoprecipitation experiments, 4×10^6 C2C12 cells were plated and lysed after 4
454 days in differentiation medium. Cells were trypsinized, washed with cold PBS, and lysed in 1
455 mL cell lysis buffer: 0.5% Tween 20, 50 mM Tris pH 7.5, 2 mM EDTA, and freshly added 1X
456 Halt protease and phosphatase inhibitor cocktail EDTA-free (Thermo, 78441). Mixture was
457 vortexed and incubated on ice for 10 min, twice. Nuclei were separated from the cytoplasmic
458 fraction by centrifugation (6000 g, 1 minute, 4°C). Nuclei were washed with 1 mL cold PBS
459 before lysing in 250 μL high salt nuclear lysis buffer: 800 mM NaCl, 1% NP40 (Igepal CA-
460 640), 50 mM Tris pH 7.5, and freshly added 1X protease and phosphatase inhibitor cocktail,
461 EDTA-free. Mixture was vortexed and incubated on ice for 10 min, twice. Nuclear lysate was
462 then diluted to a final salt and detergent concentration of 400 mM NaCl and 0.5% NP40
463 using 250 μL dilution buffer: 50 mM Tris pH 7.5 and 1X protease and phosphatase inhibitor
464 cocktail, EDTA-free. Nuclear lysates were treated with Benzonase (Merck-Millipore, 70664).
465 Nuclear lysates were pre-cleared on 25 μL Dynabeads M-280 Sheep anti-mouse or anti-
466 rabbit IgG (Thermo, 11201D/12203D), depending on primary IgG antibody. Pre-cleared
467 nuclear lysate was then added to 50 μL beads conjugated with 2-4 μg primary IgG antibody:
468 rabbit anti-APOBEC2 (Sigma, HPA017957) or rabbit IgG isotype control.
469 Immunoprecipitation was done overnight at 4°C with rotation. Beads were thoroughly washed
470 before resuspending and boiling in SDS-PAGE sample buffer.

471
472 *Immunofluorescence staining and fusion index of C2C12 cells*

473
474 C2C12 cells (5×10^4 cells) were seeded in collagen-coated coverslips (BD Biosciences,
475 356450) in 12- well plate the day before inducing of differentiation with 2% horse serum.
476 They were washed with cold PBS and fixed with paraformaldehyde (4%) in PBS for 10
477 minutes at 4 °C. This was followed by 2 washes, 5 minutes each at room temperature and
478 blocking solution (0.5% BSA, 1% gelatin, 5% normal goat serum, 0.1% Triton) in PBS for 1
479 hour at room temperature. This was followed by overnight stain with antibodies in a
480 humidified chamber at 4°C, three washes with cold PBS 5 min each at room temperature.
481 Coverslips were then incubated with secondary antibodies for 1 hour at room temperature,
482 followed by three washes with PBS 5 min at room temperature. Immunofluorescence
483 staining of C2C12 cells was carried out with primary antibodies: MyHC MF20 (DSHB) and
484 FLAG M2 (Sigma, F1804). Nuclei were counterstained and coverslips were mounted with
485 VECTASHIELD Antifade Mounting Medium with DAPI (Vector Laboratories, H-1200).
486 Images were taken using confocal Leica TCS SP5 II or widefield Zeiss Cell Observer and
487 image analysis was done with Fiji/ImageJ.

488
489 *Chromatin salt-extraction profiling*

490
491 C2C12 cells were seeded in equal numbers (2×10^6 cells) and induced to differentiate after
492 12 hours. Five days after differentiation they were lysed in the plate with 100 μl sucrose lysis
493 buffer (320 mM sucrose, 0.5% NP-40, 10 mM Tris pH 8.0, 3 mM CaCl_2 , 2 mM Mg acetate,
494 0.1 mM EDTA). Extracts were incubated for 5 minutes on ice and spun at 500 g for 5
495 minutes to collect the nuclear pellet and supernatant as the cytosol fraction. Nuclear pellets

496 were washed with no-salt Nuclei Buffer (50 mM Tris pH 8, 1% NP-40, 10% glycerol).
497 Following the washes the nuclear proteins were extracted at increasing concentrations of
498 NaCl from 250 mM up to 2 M in Nuclei Buffer during which they are homogenized using
499 dounce tissue grinders (Fisher, K8853000000), incubated on ice for 10 minutes and spun at
500 4°C for 10 additional minutes. Eluted material was collected, resolved on polyacrylamide gel
501 electrophoresis (Criterion XT Bis-Tris Gel 12%, Bio- Rad) and immunoblotted with specific
502 antibodies: Histone H4 (Merck, 05-858R), 1:5000; monoclonal mouse-APOBEC2 (clone
503 15E11, homemade), 1:5000; α -tubulin DM1A (Abcam, ab7291), 1:5000.

504

505 *RNA expression analysis*

506

507 Library preparation and sequencing were done by Rockefeller University Genomics
508 Resource Center [<https://www.rockefeller.edu/genomics/>] using TruSeq Stranded mRNA
509 Sample Prep kit as per manufacturer's instruction. The procedure includes purification of
510 poly-adenylated RNAs. Libraries were sequenced with 50bp paired-read sequencing on the
511 HiSeq2500 (Illumina). Paired end read alignments and gene expression analysis were
512 performed with the Bioinformatics Resource Center at Rockefeller University. Paired-end
513 reads were aligned to mm10 genome using the subunc function in the Bioconductor
514 Rsubread⁴⁴ package and bigWig files for visualization were generated from aligned reads
515 using the Bioconductor rtracklayer⁴⁵ and GenomicAlignments packages⁴⁶. For analysis of
516 differential expression, transcript quantifications were performed using Salmon⁴⁷ in quasi-
517 mapping mode. Gene expression values were calculated from transcript quantifications
518 using tximport⁴⁸. Gene expression changes were identified at a cut off of 5% FDR
519 (benjamini-hockberg correction) using the Wald test implemented in DESeq2⁴⁹. Annotation
520 files used: BSgenome.Mmusculus.UCSC.mm10(v1.4.0);org.Mm.db(v3.5.0);
521 TxDb.Mmusculus.UCSC.mm10.knownGene.gtf.gz(v3.4.0)

522

523 *RNA editing analysis*

524

525 RNA editing analysis was performed as previously reported elsewhere²². Editing detection
526 was performed by comparing C2C12 control samples (GFPsh) to APOBEC2 knockdown
527 samples using RNA-Seq datasets in triplicates for each sample. Minimum filters include
528 quality control thresholds (minimum of five reads covering the putative site with at least two
529 reads supporting the editing event; filtering of reads that contain indels or support an edit in
530 the first or last two base pairs of a read). Stringent filters applied to the APOBEC1
531 dependent C-to-U edited sites include all of the above and additionally the magnitude of the
532 control vector was at least 15 and the angle between the wild-type and knockout vectors was
533 at least 0.11 radians, as described in the paper referenced in this section.

534

535 *Enhanced reduced representation bisulfite sequencing (ERRBS)*

536

537 ERRBS library preparation, sequencing and read alignment was performed by the
538 Epigenomics Core Facility of Weill Cornell Medicine [epicore.med.cornell.edu/] as previously
539 described^{50,51}. The procedure includes bisulfite conversion of the DNA. Libraries were
540 sequenced with 50bp single reads (SR) in HiSeq2500 (Illumina). Reads were aligned to a
541 bisulfite converted reference mouse genome with Bismark⁵². The methylation context for
542 each cytosine was determined with scripts from the core facility.

543

544 Here coverage of specific genomic regions by ERRBS dataset, refers to the percent of
545 features (eg percent of promoters, CpG islands) that contain at least one CpG that is well
546 covered (> 10x). For gene specific annotations the mm10 UCSC knownGene annotations
547 from the UCSC table browser were used and for CpG islands the mm10 cpGIslandExt track
548 of the UCSC table browser. Genomic features were defined as: CpG islands, CpG island
549 shores were defined as 2kb upstream and downstream of a CpG island; Gene promoters

550 (region 2kb upstream and 2kb downstream of the TSS), exons, introns and intergenic
551 regions.

552

553 *Differential methylation analysis*

554

555 MethylKit (v1.3.8)⁵³ was used to identify differentially methylated cytosines (DMCs) with q-
556 value less than 0.01 and methylation percentage difference of at least 25% after filtering
557 ERRBS dataset by coverage, normalizing by median and including CpG sites that are
558 covered >10x, in 3 out of 5 biological replicates (lo.count = 10, lo.perc = NULL, hi.count =
559 1000, hi.perc = 99.9), (destrand=TRUE,min.per.group=3L). eDMRs (v0.6.4.1)⁵⁴ was used to
560 empirically determine differentially methylated regions, using the DMCs identified with
561 methylKit. In order for a region to be defined as a DMR, default parameters (num.DMCs=1,
562 num.CpGs=3, DMR.methdiff=20) of eDMR were used, so that each region has: (1) at least 1
563 DMC in the region, as determined using methylKit, (2) at least 3 CpGs included in the region
564 and (3) absolute mean methylation difference greater than 20%. For a region to be defined
565 as a significant DMR, default parameters were used (DMR.qvalue = 0.001, mean.meth.diff =
566 20, num.CpGs = 5, num.DMCs = 3) so that each significant DMRs has (1) 5 CpGs where at
567 least 3 of them are significant DMCs as determined by methylKit (2) have a minimum 20%
568 methylation change for the region.

569

570 *Chromatin immunoprecipitation method*

571

572 C2C12s were plated at ~70% confluence 12 hours prior to inducing differentiation (seed
573 ~2x10⁶ cells) maintained in DMEM (ATCC, 30-2002) with 10%FBS. This was followed by
574 media change to DMEM with 2% horse serum (Life Biotechnologies, 26050-088) to induce
575 differentiation. The cells (~5x10⁶ /10cm plate) were harvested at 24-hour or 34-hour after
576 inducing differentiation. They were fixed on plate with 1% PFA in PBS for 10 minutes at RT.
577 Glycine was added to a final concentration of 125mM. Cells were washed 2 times with 1x
578 PBS with protease inhibitor cocktail (Roche, 11836170001). They were lysed on the plate
579 with cold Farnham lysis buffer to ~10x10⁶ cells /mL (5mM PIPES pH 8.0, 0.5% NP-40,
580 85mM KCl, 1mM EDTA, PIC) and incubated rotating for 15min at 4°C . Lysates were scraped
581 off the plates, pelleted and resuspended in LB2 (10 mM Tris pH 8.0, 200 mM NaCl, 1 mM
582 EDTA, 0.5 mM EGTA, PIC) and incubated rotating for 15 minutes at 4°C and then
583 centrifuged. Pellets were resuspended to 5x10⁷ cells/mL in LB3 (10 mM Tris pH 8.0, 100
584 mM NaCl, 1 mM EDTA, 0.5 mM EGTA, 0.1% sodium-deoxycholate, 0.5% sodium lauroyl
585 sarcosinate, PIC) until suspension was homogenized. Samples were then sonicated using
586 Covaris ultrasonicator model S220 for 15 minutes with the following settings: 140W peak
587 power, 5% duty, 200 cycles per burst. TritonX-100 to a final concentration of 1% was added
588 to the samples. Samples were clarified by centrifugation at 20,000 g for 10 minutes at 4°C.
589 The supernatant is the soluble chromatin extract. The soluble fragmented chromatin from
590 ~2.5x10⁷ was used for each IP. For each IP 100ul Dynabeads (ThermoFisher anti-rabbit
591 M280, 11203D) were mixed with 10ul polyclonal rabbit-APOBEC2 antibodies (gift from Alin
592 Vonica MD, PhD) incubating overnight (~16 hours). A magnetic stand was used to separate
593 beads from the lysate and beads were washed one time each with for 5min in: low salt wash
594 (0.1%SDS, 1%Triton X-100, 2 mM EDTA, 20 mM Tris pH8, 150 mM NaCl, PIC), high salt
595 wash (0.1%SDS, 1% Triton X- 100, 2mM EDTA, 20mM Tris pH8, 500mM NaCl, PIC), lithium
596 chloride wash (150mM LiCl, 1% NP-40, 1% NaDOC, 1mM EDTA, 10mM TrispH8, PIC), TE
597 wash (10mM Tris-HCl pH8, 1mM EDTA, 50mM NaCl, PIC). Beads were resuspended in 52
598 ul of elution buffer (50mM Tris-HCl pH8, 10mM EDTA, 1%SDS) and incubated at 30min at
599 65°C while shaking to prevent beads from settling. The eluate was transferred to a new tube,
600 inputs of the same volume were incubated for 8 hours at 65°C to reverse the crosslink. The
601 samples were treated with RNase (Roche, 11119915001) for 1 hour at 37°C, and with
602 Proteinase K for 2 hours at 55°C. Fragmented DNA was purified with Ampure beads
603 (Agencourt AMPure XP beads A63881) as per the manufacturer's instructions.

604

605 *Chromatin immunoprecipitation sequencing and analysis*

606

607 The ChIP-Seq included biological triplicates for each group. ChIP-Seq libraries were
608 prepared using NEBNext Ultra DNA Library Prep Kit as per manufacturer's instructions.
609 Libraries were sequenced with 75 base pair single read sequencing on the NextSeq 500
610 (Illumina). Read alignments and initial analysis were performed with the Bioinformatics
611 Resource Center at Rockefeller University. Single-end reads were aligned to mm10 genome
612 using the subread function in the Bioconductor Rsubread⁴⁴ package and bigWig files for
613 visualization were generated from aligned reads using the Bioconductor rtracklayer⁴⁵ and
614 GenomicAlignments packages⁴⁶. Quality metrics for the ChIP-Seq data were assessed
615 using ChIPQC bioconductor package⁵⁵, according to Encyclopedia of DNA Elements
616 (ENCODE) working standards and guidelines for ChIP experiments⁵⁶. Reads mapping to
617 more than one genomic location were filtered prior to peak calling using Model-based
618 Analysis of ChIP-Seq (MACS2)^{57,58} with duplicate filtering applied and input DNA sample as
619 a control. Peaks that are reproducible (present in 2 out of 3) were filtered for known artifact
620 or blacklisted regions (The ENCODE Project Consortium, 2012). For each of the peaks a
621 weighted mean location of peak summits cross biological replicates is calculated⁵⁹. The list
622 of binding regions 100 base pairs around the mean peak summits was used for downstream
623 analysis. Ngs.plot (v2.61) was used with specific parameters (-G mm10 -D refseq -C -L 1000
624 -FL 150 -P 4 -SC 0,1 -GO none -RB 0.05) to generate average profiles of ChIP-Seq reads
625 (Shen et al., 2014). ChIPSeeker (v1.14.2)⁶⁰ and ChIPpeakAnno (3.12.7)^{61,62} were used for
626 downstream analysis after peak calling for annotation of the binding regions to the nearest
627 gene. We created an APOBEC2 occupied gene set, using genes that show consistent
628 APOBEC2 occupancy at both 14-hour and 34-hour time points. GSEA (v3.0)⁶³ was used for
629 testing the enrichment of the APOBEC2 occupied gene set in the list of genes that are
630 differentially expressed. Annotation files used: BSgenome.Mmusculus.UCSC.mm10 (v1.4.0)
631 org.Mm.db (v3.5.0) and TxDb.Mmusculus.UCSC.mm10.knownGene.gtf(v3.4.0).

632

633 *Gene list analysis*

634

635 Gene list analyses either by statistical overrepresentation test or statistical enrichment test
636 were done through PANTHER⁶⁴. Briefly, gene lists were filtered based on expression
637 (\log_2 FoldChange, up- or downregulated at specific treatment and time point) and p-adj
638 values (FDR < 10%) and used as input in PANTHER gene list analysis. For statistical
639 overrepresentation tests of upregulated genes with A2 vs GFP shRNA, genes were filtered
640 based on \log_2 FoldChange > 0.58 and FDR < 10% at each time point and used as input list
641 with Mus musculus (all genes in database) as reference/background list. Default parameters
642 were followed for the analyses and are indicated in the corresponding output. For

643

644 *Prediction of binding motifs*

645

646 Transcription factor motifs associated to 108 TF modules²⁹ were mapped against time-point
647 specific sequences harboring APOBEC2, 200 base pairs centered on peak summits. For
648 each time point, we defined a background set of negative sequences using scrambled
649 regions of the positive sequences. Using both sequence sets of positives and negatives, we
650 assessed the presence of strong 8-mers associated to each of those 108 families and their
651 ability to classify between APOBEC2 regions and negative sequences, summarizing a
652 Receiver-Operating Characteristic Area Under the Curve (ROC-AUC) for each of those.
653 Assessment of significance in each case was done using a Wilcoxon rank sums test (one
654 sided). P-values were corrected through a Benjamini-Hochberg procedure.

655

656 *Enrichment of ChIP-seq peaks on APOBEC2 differentially expressed target genes*

657

658 Using the ChIP-Atlas as a reference, we downloaded all datasets associated to myoblast or
659 C2C12 cells (N=54). For each dataset, we intersected ChIP-seq peaks from APOBEC2 in

660 each timepoint and replicate (command *fisher* in *bedtools*), obtaining a 2 x 2 contingency
661 matrix. The number of overlaps was linked to the closest gene using 2000bp with respect to
662 TSS annotations in the mouse genome. The proportion of genes associated to a differential
663 expression comparison was done by dividing the number of APOBEC2 peaks proximal to a
664 DE-gene with a peak from a ChIP-Atlas dataset by the total number of DE-genes in that
665 comparison. This was repeated for each gene expression contrast. Mean log₂ fold change
666 estimates for each ChIP-Atlas peak dataset were obtained by calculating the distribution of
667 log₂ fold changes between non-target DE-genes and target DE-genes, in each time point,
668 using the three APOBEC2 ChIP-seq replicates. With those, we calculated a global mean and
669 standard deviation across all ChIP-Atlas factors, reporting a Z-score for dataset, time point
670 and differentially expression comparison between APOBEC2 target and non-target genes.

671

672 *BioID samples preparation*

673

674 Constructs encoding mouse APOBEC2 fused to BirA-Flag by the N- and C-terminus were
675 cloned into pMX-puro. Both constructs, as well as the eGFP-BirA-Flag control, were modified
676 to encode a weak Kozak sequence (TATTGTATG) to reduce protein expression levels.
677 Virions containing the pMX vectors were produced in the Plat-E packaging cell line⁶⁵.
678 C2C12 cells were spininfected with Plat-E supernatant, 8mg/ml polybrene (16,000 rpm, 90
679 min, 30C) and selected with 4 µg/ml puromycin to obtain stable cell populations. Similar bait
680 and control expression levels were confirmed by western blot, and localization of the
681 APOBEC2 constructs analyzed by immunofluorescence. C2C12 cells expressing each
682 construct were pre-cultured for 24 h with 2% low horse serum before supplementing the
683 media to 50 µM biotin (BioBasic). Cells were harvested 24 h later, washed 3× with PBS, then
684 lysed in 1.5 mL of RIPA buffer and sonicated 30 s at 30% amplitude (3 × 10 s bursts with a
685 2 s break in between). Benzonase (250 U, Sigma) was added to the lysates during
686 centrifugation, 30 min at 16,000 × g, 4 °C. Forty µL aliquots of supernatant were kept to
687 monitor expression and biotinylation and run on western blot, and the remaining lysate was
688 incubated with 70 µL of pre-washed streptavidin-sepharose beads (Sigma) for 3 h on a
689 rotator at 4 °C. Beads were then washed with 1 mL of RIPA buffer, transferred to a new tube
690 and washed again 2× with 1 mL of RIPA buffer and then 3× with 1 mL of 50 mM Ammonium
691 Bicarbonate (ABC) (Biobasic). Beads were then resuspended in 100 µL of ABC with 1 µg of
692 trypsin (Sigma) and incubated overnight at 37 °C with rotation. The following day, 1 µg of
693 trypsin was added for a further 2 h digestion. Samples were centrifuged 1 min at 2000 RPM,
694 and the supernatant was transferred to a new tube. Beads were rinsed twice with 100 µL of
695 water, and all supernatants were pooled and adjusted to 5% formic acid. Samples were then
696 centrifuged for 10 min at 16,000 × g for clarification. Trypsin-digested peptides in the
697 supernatant were dried in a SpeedVac (Eppendorf) for 3 h at 30 °C. Samples were
698 resuspended in 15 µL of 5% formic acid and kept at -80 °C for mass spectrometric analysis.

699

700

701 *BioID MS Data analysis*

702

703 Mass spectrometry was performed at the IRCM proteomics platform. Samples were injected
704 into Q Exactive Quadrupole Orbitrap (Thermo Fisher), and raw files were analyzed with the
705 search engines Mascot and XTandem!⁶⁶ through the iProphet pipeline⁶⁷ integrated in
706 Prohits⁶⁸, using the mouse RefSeq database (version 73) supplemented with "common
707 contaminants" from the Max Planck Institute (<http://maxquant.org/downloads.htm>), the
708 Global Proteome Machine (GPM; <http://www.thegpm.org/crap/index.html>) and decoy
709 sequences. The search parameters were set with trypsin specificity (two missed cleavage
710 sites allowed), variable modifications involved Oxidation (M) and Deamidation (NQ). The
711 mass tolerances for precursor and fragment ions were set to 15 ppm and 0.6 Da,
712 respectively, and peptide charges of +2, +3, +4 were considered. Each search result was
713 individually processed by PeptideProphet⁶⁹, and peptides were assembled into proteins
714 using parsimony rules first described in ProteinProphet⁷⁰ using the Trans-Proteomic

715 Pipeline (TPP). TPP settings were the following: -p 0.05 -x20 -PPM -d "DECOY", iprophet
716 options: pPRIME and PeptideProphet: pP.

717

718 *BioID interactions scoring*

719

720 Six biological replicates of each bait and paired eGFP controls were done in two
721 independent experiments (3 replicates each) and combined for the analysis for maximal
722 statistical power. The estimation of interactions scorings was performed for proteins with
723 iProphet protein probability ≥ 0.9 and unique peptides ≥ 2 , by combining two algorithmic
724 approaches : SAINTexpress⁷¹ and DESeq⁷². The SAINTexpress (version 3.6.1) analysis
725 was performed with default settings using no compression for controls or baits. Interactions
726 displaying a BFDR ≤ 0.01 were considered statistically significant. We also used DESeq2
727 (version 1.2.1335), an R package that applies negative binomial distribution to calculate
728 enrichments over controls. DESeq was run using default settings and significant preys were
729 selected by applying a ≤ 0.1 p-value cut-off. The combined list of significant preys obtained
730 from DESeq and SAINT was defined as potential APOBEC2 proximity interactors.

731

732 *BioID annotations and network analyses*

733

734 Graphical representations of protein networks were generated with Cytoscape⁷³ (version
735 3.8.2). Prior to the importation of APOBEC2's network in Cytoscape, mouse to human
736 orthologs were extracted from the Ensembl database with the BioMart export tool (Mouse
737 genes version GRCm38.p6). Next, we extracted human prey-prey interactions from BioGrid
738 release 4.2.192⁷⁴ and from Cytoscape's PSICQUIC built-in web service client (April 2021
739 release) by searching against the IntAct database⁷⁵. Once augmented, clusters were
740 extracted with the Markov CLustering Algorithm (MCL) from Cytoscape's ClusterMaker2
741 application (version 1.3.1)⁷⁶. To identify relevant complexes among clusters, the APOBEC2
742 interactome was annotated with the Gene Ontology Annotation database⁷⁷ (GOA version
743 171) and CORUM (version 3.0)⁷⁸, a database of known protein complexes.
744 EnrichmentMaps⁷⁹ of GO Biological Processes were generated by importing g:Profiler's⁸⁰
745 generic enrichment file outputs and mouse GO BP GMT file. p-values ≤ 0.05 and q-value \leq
746 0.05 were set as node cutoffs, and Edge cutoff (similarity) were set at 0.345.

747 *DNA editing detection*

748

749 We aligned all short reads from input and IP experiments to the mouse genome (GRCm38
750 EnsEMBL 90) using HiSAT v2.1.0 with default settings. We removed all non-unique mappers
751 and marked all read duplicates with picard.sam.markduplicates.MarkDuplicates (v 2.5.0). We
752 compared all samples to the reference genome using JACUSA v1.2.4 in call-1 mode with
753 program parameters: call-1 -s -c 5 -P UNSTRANDED -p 10 -W 1000000 -F 1024 --
754 filterNM_1 5 -T 1 -a D,M,Y -R. Diverging positions are reported if the LLR ratio exceeds 1.0.
755 Briefly, read count distributions at every genomic position (coverage >5) are contrasted with
756 the expected read count based on the reference base. For the pairwise comparison of all
757 input samples stratified by conditions, we used JACUSA v.1.2.4 in call-2 mode with program
758 parameters: call-2 -s -c 5 -P UNSTRANDED,UNSTRANDED -p 10 -W 1000000 -F 1024 --
759 filterNM_1 5 --filterNM_2 5 -T 1 -a D,M,Y -u DirMult:showAlpha -R. Briefly, read count
760 comparison from replicate input samples are contrasted with one another: A2 shRNA
761 knockdown vs GFP shRNA knockdown. Diverging positions are reported if the LLR ratio
762 exceeds 1.0.

763

764 *Recombinant mouse APOBEC2 production*

765 Recombinant His₆-tagged mouse APOBEC2 proteins were produced in Sf21 insect cells by
766 the EMBL Protein Expression and Purification Core Facility. The genes encoding mouse
767 APOBEC2 were cloned into the pFastBac HTa vector (Thermo) and these constructs were

768 used for transposition into *E. coli* DH10EMBacY cells (Geneva Biotech). The isolated bacmid
769 DNA was utilised for generation of the recombinant baculoviruses. For the mouse APOBEC2
770 protein production, 5 mL of baculovirus was used to infect 1 L of Sf21 cells at a density of $1 \times$
771 10^6 cells/ml. After 72h, the cells were harvested by centrifugation (30 min, 600 x g, 4°C) and
772 resuspended in lysis buffer (20 mM Tris pH 8.0, 800 mM NaCl, 20 mM imidazole and 5 mM
773 β -mercaptoethanol) supplemented with benzonase, 10 mM MgCl₂ and cOmplete EDTA-free
774 protease inhibitors (Roche). The cells were lysed using a Dounce homogenizer and the
775 lysate was cleared by centrifugation (30 min, 20000 x g, 4°C). The cleared lysate was
776 loaded onto a 5 mL Ni-NTA column (Macherey-Nagel). After washing with a buffer consisting
777 of 20 mM Tris pH 8.0, 300 mM NaCl, 20 mM imidazole and 5 mM β -mercaptoethanol, the Ni-
778 NTA column was eluted using a gradient up to 300 mM imidazole. The elution fractions
779 containing mouse APOBEC2 were pooled and dialysed overnight at 4°C to ion exchange
780 buffer (20 mM Tris pH 8.0, 100 mM NaCl, 1 mM DTT). The dialysed sample was loaded onto
781 a 5 mL HiTrap Heparin HP column (Cytiva) coupled to a 5 mL HiTrap Q HP anion exchange
782 column (Cytiva). After washing, the HiTrap Heparin HP column and the HiTrap Q HP column
783 were eluted separately in a gradient ranging from 100 mM to 1M NaCl. Finally, the mouse
784 APOBEC2 protein eluted from the HiTrap Q HP column was subjected to a size exclusion
785 chromatography (SEC) step using a HiLoad 16/600 Superdex 75 pg column (Cytiva) pre-
786 equilibrated with SEC buffer (20 mM HEPES pH 7.5, 150 mM NaCl and 0.5 mM TCEP).
787 When removal of the His₆-tag was required, His₆-tagged TEV protease (produced in-house)
788 was added to the purified mouse APOBEC2 protein. After the overnight TEV cleavage step
789 at 4°C, Ni-NTA beads (Qiagen) were added to the sample and incubated for 1h at 4°C. After
790 centrifugation (1 min, 100 x g, 4°C), untagged mouse APOBEC2 was recovered from the
791 flow through of the Ni-NTA beads. Recombinant mouse APOBEC2 proteins were aliquoted,
792 flash-frozen with liquid N₂ and stored at -80°C. *Microscale Thermophoresis (MST)*

793
794 Purified APOBEC2 was labeled using Cy5 Mono NHS Ester (GEPA15101, Sigma-Aldrich) at
795 5 mg/mL protein and a 3:1 dye:protein ratio. Labeling reactions were performed in 20 mM
796 HEPES, pH 7.5, 150 mM NaCl, and 0.5 mM Tris(2-carboxyethyl)phosphine (TCEP).
797 Reactions were incubated overnight at 4°C with constant agitation. After incubation,
798 reactions were deactivated using quencher buffer (ab102884, Abcam). Remaining dye was
799 washed away by concentrating protein using Vivaspin® 500 centrifugal concentrators
800 (Sartorius) into MST buffer (10 mM HEPES pH 7.5, 50 mM NaCl, 5 mM MgCl₂). The degree
801 of labeling was typically at about 1.

802
803 Oligonucleotides (oligos) were ordered from Sigma-Aldrich: SP/KLF motif F: GGC GGC
804 GCG GCC CCG CCC CCT CCT CCG GC; SP/KLF motif R: GCC GGA GGA GGG GGC
805 GGG GCC GCG CCG CC; A-tract motif F: TCT CAA GAA AAA AAA AAA AAG AC; A-tract
806 motif R: GTC TTT TTT TTT TTT TCT TGA GA.

807
808 Oligonucleotides were annealed by incubating at 95°C and slow cooling to 25°C before
809 storing at 4°C. Oligonucleotides were diluted to MST buffer + 0.05% Tween-20 for the final
810 reaction. MST buffer was supplemented with 0.05% Tween-20. Cy5-labeled APOBEC2 was
811 held constant at 50 nM while the oligonucleotides were titrated (1:1 dilution) between 19.53
812 to 20,000 nM. Reactions were incubated for 30 min before loading into standard glass
813 capillaries (MO-KO22, NanoTemper Technologies). MST measurements were performed
814 using a Monolith NT.115 (NanoTemper Technologies) at 85% LED power and 40% MST
815 power. Data represent 3 independent measurements. MO.Affinity Analysis v2.1.3454
816 (NanoTemper Technologies) was used for curve fitting and calculating K_d values with
817 Thermophoresis + T Jump settings.

818
819 *Electromobility shift assay (EMSA)*

820
821 Oligos used for MST were labeled with [γ -³²P] ATP and annealed with complementary oligos
822 to form double-stranded (ds) oligos. Specified recombinant protein, mouse APOBEC2 and/or

823 human SP1 (Sigma, SRP2030), and ss or ds oligos were mixed in binding reaction buffer
824 (10 mM HEPES pH 7.5, 50 mM NaCl, 5 mM MgCl₂, 5% glycerol and 5 mM DTT) for 30
825 minutes at room temperature. Reactions were resolved on 5% TBE gel (3450048, BioRad)
826 with 0.5X TBE buffer (1610733, Bio-Rad) for 1.5 hours at 120 volts with the tank submerged
827 on ice. Gels were then dried and imaged with a phosphorimager system (Azure Biosystems,
828 Inc.).

829

830 **Acknowledgements**

831

832 The authors thank Dr. Diego Mourao-Sa for his insights and support during the completion of
833 these studies; Dr. Thomas Carroll, for reproducing RNA-Seq and ChIP-Seq bioinformatics
834 analyses; Dr. Pete Stavropoulos, Erik Debler, Philipp Schmiege and Nicholas Economos for
835 initially producing APOBEC2 protein and mouse monoclonal (15e11) antibody; Dr. Frank
836 Schwarz and GPCF@DKFZ for assistance with the MST experiments. We would like to
837 thank Julia Flock and Dr. Kim Remans (Protein Expression and Purification Core Facility,
838 EMBL) for producing the recombinant mouse APOBEC2 in Sf21 insect cells. Last but not
839 least, FNP and LM would like to thank Dr Bruce McEwen (1938-2020) and Dr Karen Bulloch.
840 Without their lasting support and encouragement this work would not have been completed.

841

842 **Funding**

843

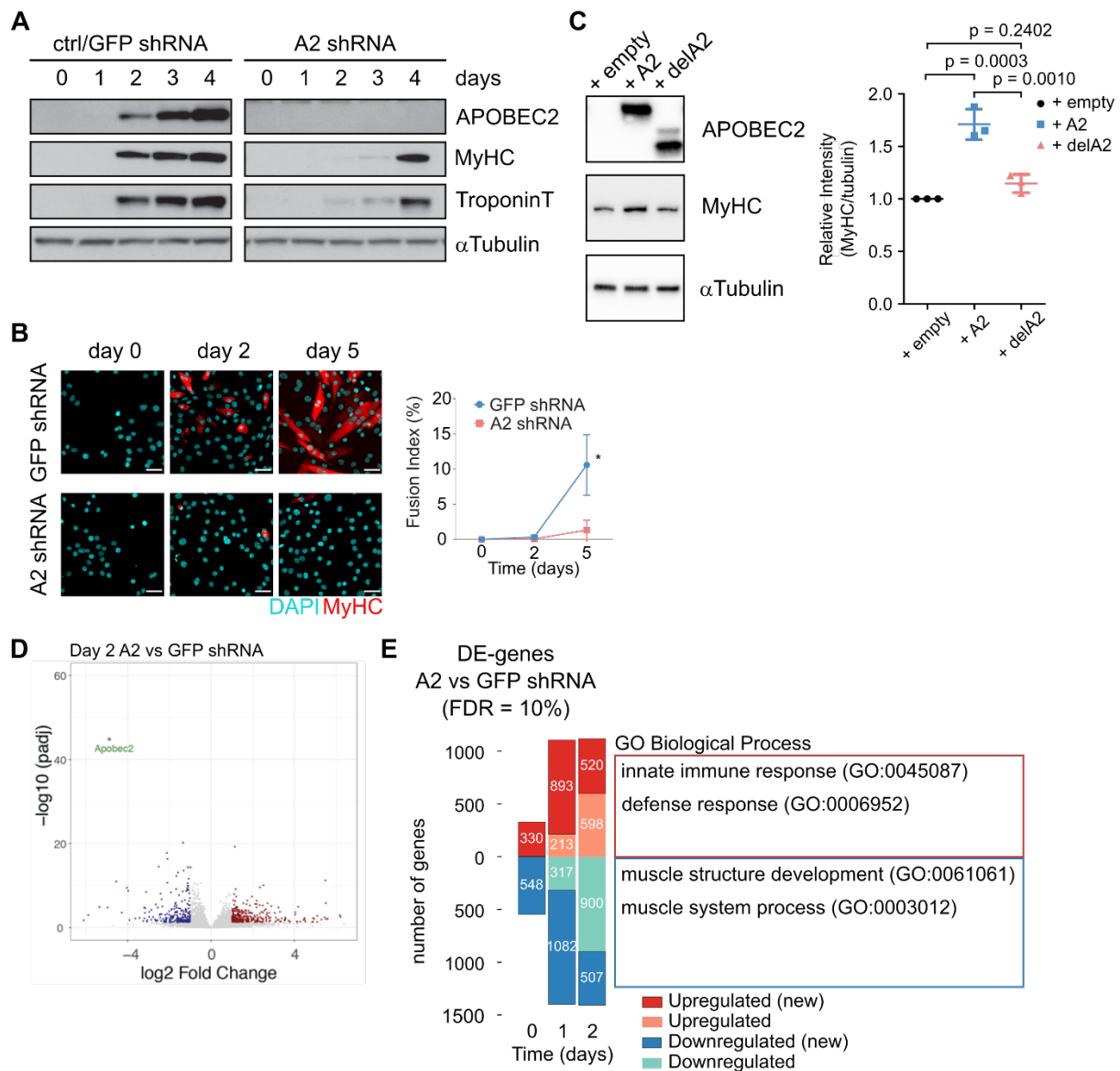
844 This work is supported through funding by the Helmholtz Foundation to the DKFZ (FNP).
845 Financial support was provided through the David Rockefeller Graduate Program (LM). Work
846 in the JMDN lab is supported by the Canadian Institutes of Health Research grant PJT
847 155944.JMDN in a merit scholar from The Fonds de recherche du Québec – Santé.
848

849 **Author Contribution**

850 LM and JPL designed the study, performed experiments, analyzed data, and wrote the
851 manuscript with supervision from FNP. SR for performing supplementary experiments. DH
852 performed RNA editing analysis. ILR performed motif prediction and enrichment of ChIP-seq
853 peaks analysis with supervision from JBZ. PGS and JR performed experimental work and JB
854 performed analysis related to BioID data with supervision from JMDN. AV provided key
855 reagent. CD performed DNA editing detection analysis. All authors wrote, read, and
856 approved the final manuscript.

857

Figure 1



858

859 **Figure 1. APOBEC2 expression is required for myoblast differentiation**

860 **(A)** Cell lysates from C2C12 cell lines, ctrl/GFP shRNA and A2 shRNA, at different
 861 timepoints of myoblast differentiation (day 0 to day 4) were analyzed by Western blot.
 862 C2C12 myoblasts were transduced either with shRNA against GFP (ctrl/GFP shRNA) or
 863 shRNA against APOBEC2 (A2 shRNA). MyHC (myosin heavy chain) and TroponinT were
 864 used as markers of late differentiation; α Tubulin, as loading control.

865

866 **(B)** C2C12 cell lines were fixed and immunostained using an antibody specific to MyHC
 867 (red), DAPI (cyan) was used to stain for DNA. Scale bar = 50 μ m. Line plot shows
 868 quantification of fusion index. Statistics: t test. Six fields of view were measured, and data is
 869 shown as means (n = 3). Error bars indicate SD; * = $p < 0.05$.

870

871 **(C)** C2C12 knockdown cell line (A2 shRNA) was transduced with retrovirus overexpressing
 872 APOBEC2 or empty vector (+ empty: transduced with empty vector, + A2: with
 873 APOBEC2 vector, and + delA2 with truncated APOBEC2). Cells were collected 96 hours
 874 post-transduction. Cell lysates were prepared and analyzed by Western blot. Representative
 875 blot from 3 independent biological replicates. Statistics: Ratio of MyHC mean intensity to
 876 α Tubulin was normalized to corresponding + empty sample for each trial. Dot plot represent

877 mean with error bars representing standard deviation (n = 3). One-way ANOVA with Tukey's
878 multiple comparisons test was performed to calculate p (adjusted P value).

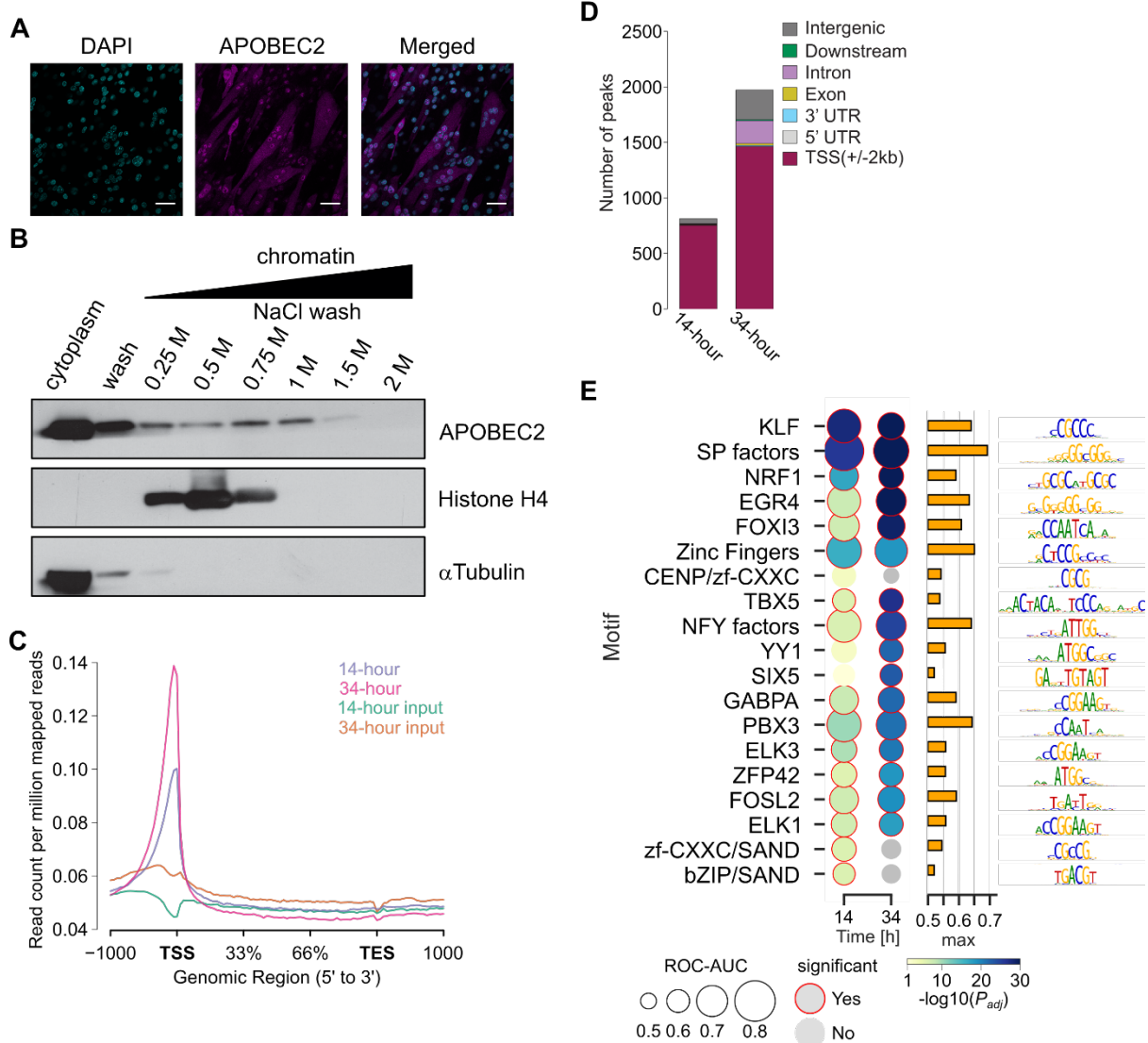
879

880 **(D)** Volcano plot was generated using log₂ fold changes and p-adjusted values from
881 comparing gene expression differences due to APOBEC2 knockdown at day 2 following
882 induction of differentiation. Significantly differentially expressed genes with p adjusted value
883 <0.05 are shown in red (upregulated) or blue (downregulated) and not significantly
884 differentially expressed genes in gray. APOBEC2 is shown in green.

885

886 **(E)** Number of differentially expressed genes (DE-genes) between APOBEC2 knockdown
887 (A2 shRNA) relative to GFP shRNA control. Colors indicate up- (red) and down-regulated
888 (blue) genes. A false discovery rate (FDR) cutoff of 10% was used to determine DE-genes.
889 Dark red and blue indicate newly differentially expressed genes at a given time point.
890 Common GO Biological Process terms across day 0 to 2 from statistical enrichment test
891 ranking genes by log₂FoldChange (see Supplementary File 1 for complete output tables of
892 the tests).

Figure 2



893
894
895
896
897

Figure 2. APOBEC2 localization and ChIP-Seq in differentiating C2C12 myoblasts.
(A) Immunostaining of APOBEC2 (magenta) and DAPI-positive (blue) nuclei in differentiated C2C12 myoblasts (5 days in differentiation medium). Scale bar = 50 μ m.

(B) The sequential salt extraction profile of endogenous APOBEC2 and histone H4 are shown. alpha-tubulin is a cytoplasmic marker. The amount of indicated proteins in eluates was measured by Western blotting.

(C) The mean normalized APOBEC2 signal (plotted as read counts per million mapped reads) across all annotated genes. This plot shows the global differences in APOBEC2 binding between the two time points in TSS. Both time points are in biological triplicates.

(D) Genomic annotations of APOBEC2 consensus binding regions in each of the time points (14- and 34-hour). Binding regions are annotated based on genomic feature. The priority of assignment to a genomic feature when there is annotation overlap is: Promoter (2kb around the TSS), 5' UTR, 3' UTR, Exon, Intron, Downstream (within 3kb downstream of the end of the gene).

(E) Enrichment of 8-mers associated to 19 known transcription factors specificities (motifs) in APOBEC2 ChIP-seq regions, compared against negative genomic regions (see Methods). Receiver Operating Characteristic Area under the Curve (ROC-AUC, circle sizes) values are

915 descendently sorted on the y-axis by minimum adjusted P value observed in both time points
916 (color). All 18 shown transcription factors are significant on at least one time point (adjusted
917 P value < 0.1, using one-sided Wilcoxon rank sum test and Benjamini-Hochberg correction.
918 Red circles). Right barplot indicates maximum ROC-AUC value, row-wise. Right sequence
919 logos depict unsupervised alignment of all 8-mers referred to that transcription factor motif ²⁹.

Figure 3

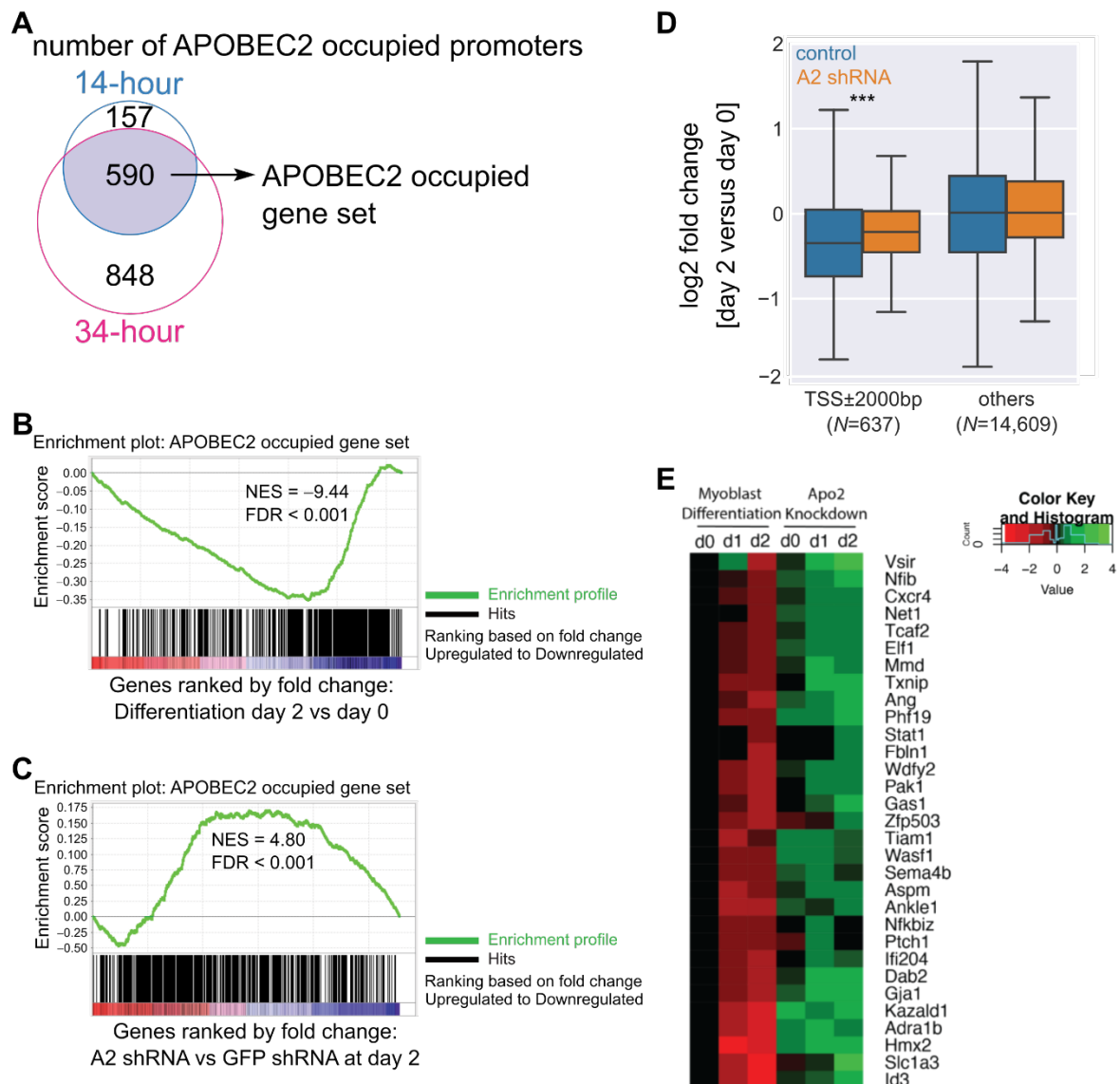


Figure 3. APOBEC2 binding at specific transcription factor DNA motifs.

(A) The Venn diagram represents the number of genes that have APOBEC2 occupancy on their promoters at 14- and 34-hour time points. The genes that show consistent APOBEC2 occupancy in their promoters at both time points were used to create an APOBEC2 occupied gene set as shown in the Venn diagram.

(B,C) Gene set enrichment analysis (GSEA) (Subramanian et al., 2005) was used to test the enrichment of the APOBEC2 occupied gene set in the list of genes that are differentially expressed through differentiation (C) or the ones that are differentially expressed due to APOBEC2 knockdown at day 2 (D). The enrichment profile over the whole ranked gene set is shown in green with normalized enrichment score (NES) and FDR values. Gene hits are shown as black lines. A positive NES indicates gene set enrichment at the top (positive/up fold change) of the ranked list; a negative NES indicates gene set enrichment at the bottom (negative/down fold change) of the ranked list.

(D) Expression changes for genes in control (GFP control shRNA) and A2 knockdown (A2 shRNA) C2C12 during differentiation. Genes are grouped by the presence of an APOBEC2

920
921

922

923

924

925

926

927

928

929

930

931

932

933

934

935

936

937

938

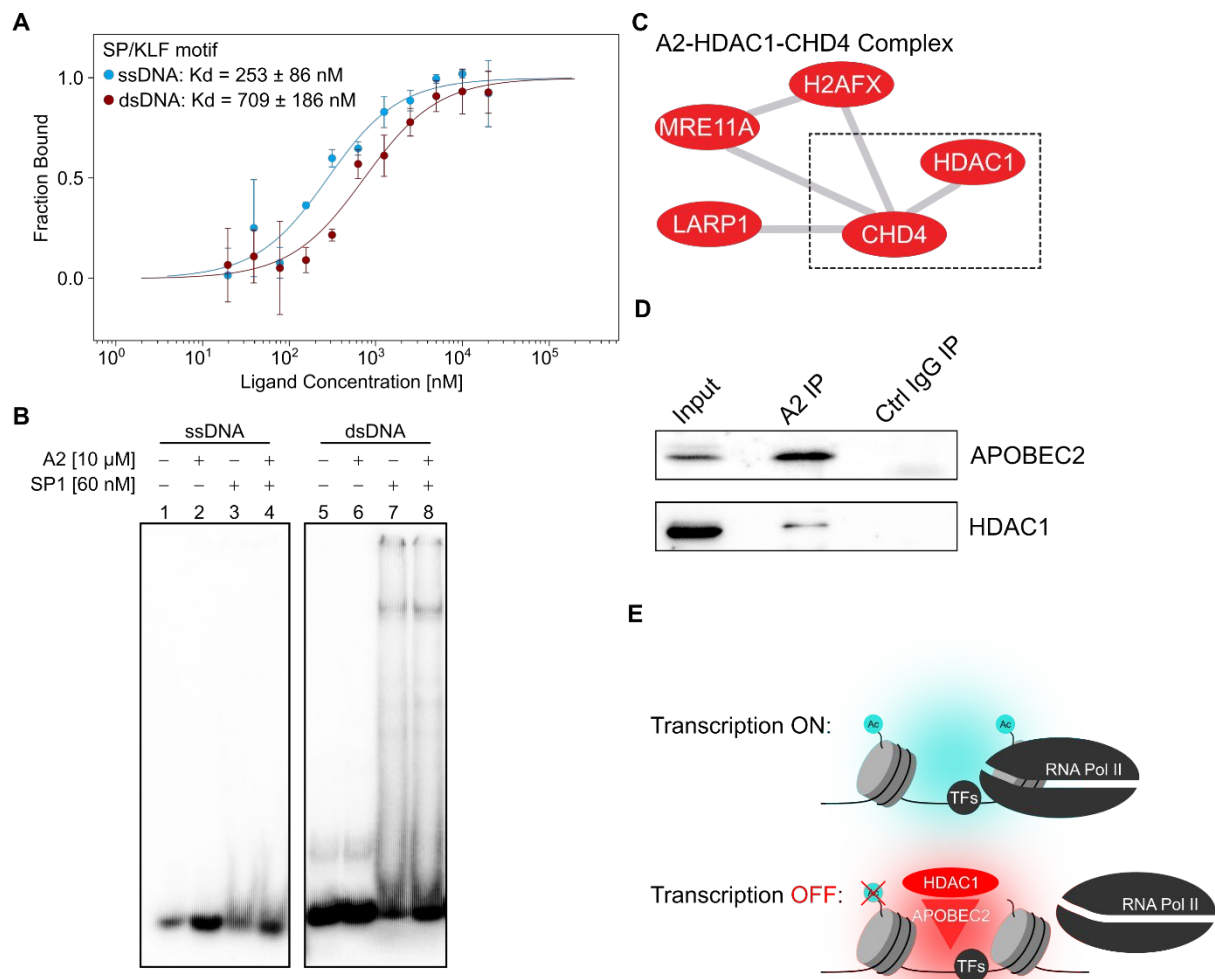
939

940 ChIP-seq peak nearby Transcription Start Sites (TSS) at not more than 2000bp from it, or
941 genome wide background (others). Asterisks indicate adjusted P values, by two-sided t-test
942 corrected using Benjamini Hochberg procedure (***=0.001).

943

944 **(E)** Heatmap showing expression changes of genes related to differentiation (regulation of
945 differentiation, GO: 0045595) occupied by A2 during differentiation in C2C12 cells and A2
946 knockdown cells. The list of APOBEC2 repressed genes were filtered from the C2C12
947 RNASeq data of A2 occupied genes (defined as genes with A2-ChIPSeq peak in the
948 promoter region). Genes repressed during differentiation log₂ fold change greater than 0.58
949 (absolute fold change > 1.5) at day 1 or 2 of differentiation and upregulated in the
950 knockdown (versus control) at day 0, 1, or 2 were selected. These genes were then used as
951 input for statistical overrepresentation test – GO biological processes through Panther (ver
952 14) with the default settings using all *M. musculus* genes in database as reference list⁸¹.

Figure 4



953

954

955 **Figure 4. APOBEC2 recruits the HDAC1 co-transcriptional repressor complex.**

956 **(A)** Microscale thermophoresis (MST) experiments measuring purified APOBEC2 binding to
 957 single-stranded DNA (ssDNA) or double-stranded (dsDNA) SP/KLF motif. Cy5-labeled
 958 APOBEC2 was kept constant (50 nM) while the concentration of non-labeled SP/KLF motif
 959 was titrated (1:1 dilution) between 20 nM – 20,000 nM. The calculated K_d was computed
 960 using the standard settings (thermophoresis + T jump) with the MO.Affinity Analysis v2.1
 961 (NanoTemper Technologies). Values represent 3 independent measurements with error
 962 bars representing the standard deviation.

963

964 **(B)** Electrophoretic mobility shift assays (EMSA) of recombinant mouse APOBEC2 and
 965 human SP1 protein on either ss or dsDNA with an SP/KLF motif. Radioactively labeled ss or
 966 dsDNA (1 nM) was mixed with either recombinant APOBEC2 (10 μ M) or SP1 (60 nM)
 967 protein, or both. Gel shift image is representative of at least 3 independent experiments.

968

969 **(C)** Selected protein complex identified by APOBEC2 proximity-dependent protein
 970 biotinylation (BioID). Each red node corresponds to a protein that was identified by BioID
 971 mass spectrometry to interact with APOBEC2. CHD4 was also identified in a BioID data
 972 comparing APOBEC2 and AID in mouse B cells⁸². The edges denote the known interactions
 973 of these proteins with each other (see Figure S5B for other complexes).

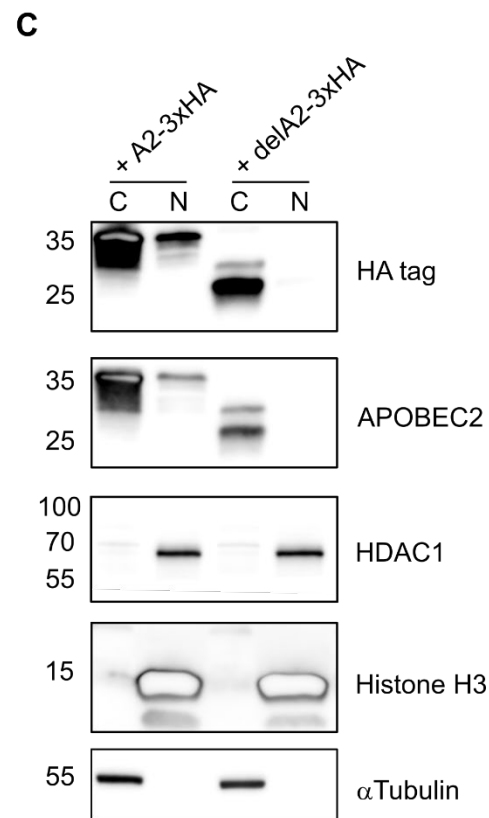
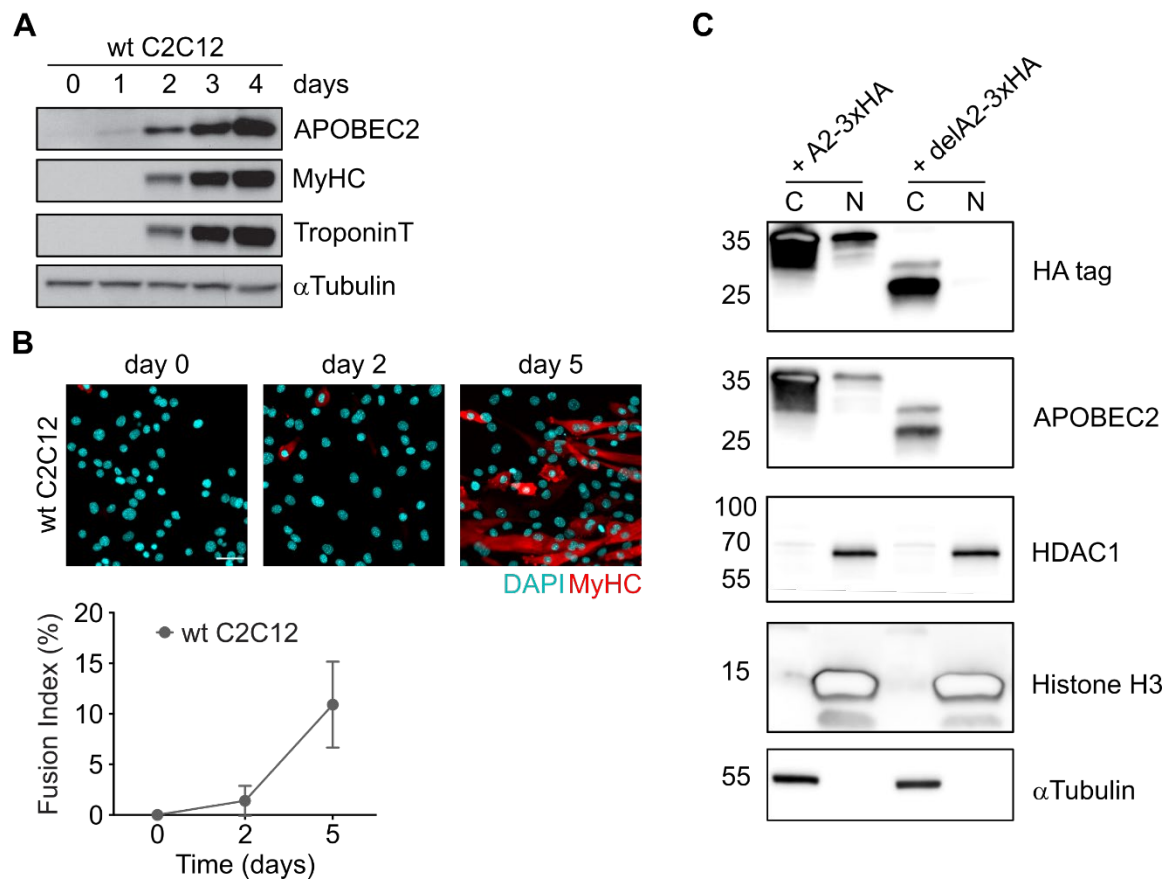
974 **(D)** Co-immunoprecipitation (Co-IP) of APOBEC2 with HDAC1 in C2C12 myoblasts
 975 differentiated to myotubes for 4 days. Nuclear protein lysates (Input) were incubated with

976 beads conjugated to either APOBEC2 antibody (A2 IP) or IgG isotype control antibody (Ctrl
977 IgG IP). Proteins were then eluted, ran on an SDS-PAGE gel, and blotted with APOBEC2, or
978 HDAC1 antibodies.

979

980 **(E)** Proposed molecular function of APOBEC2 as a co-transcriptional repressor complex that
981 acts on active/open chromatin to repress transcription through HDAC1 histone deacetylation
982 during myoblast differentiation.

Figure S1



983
984

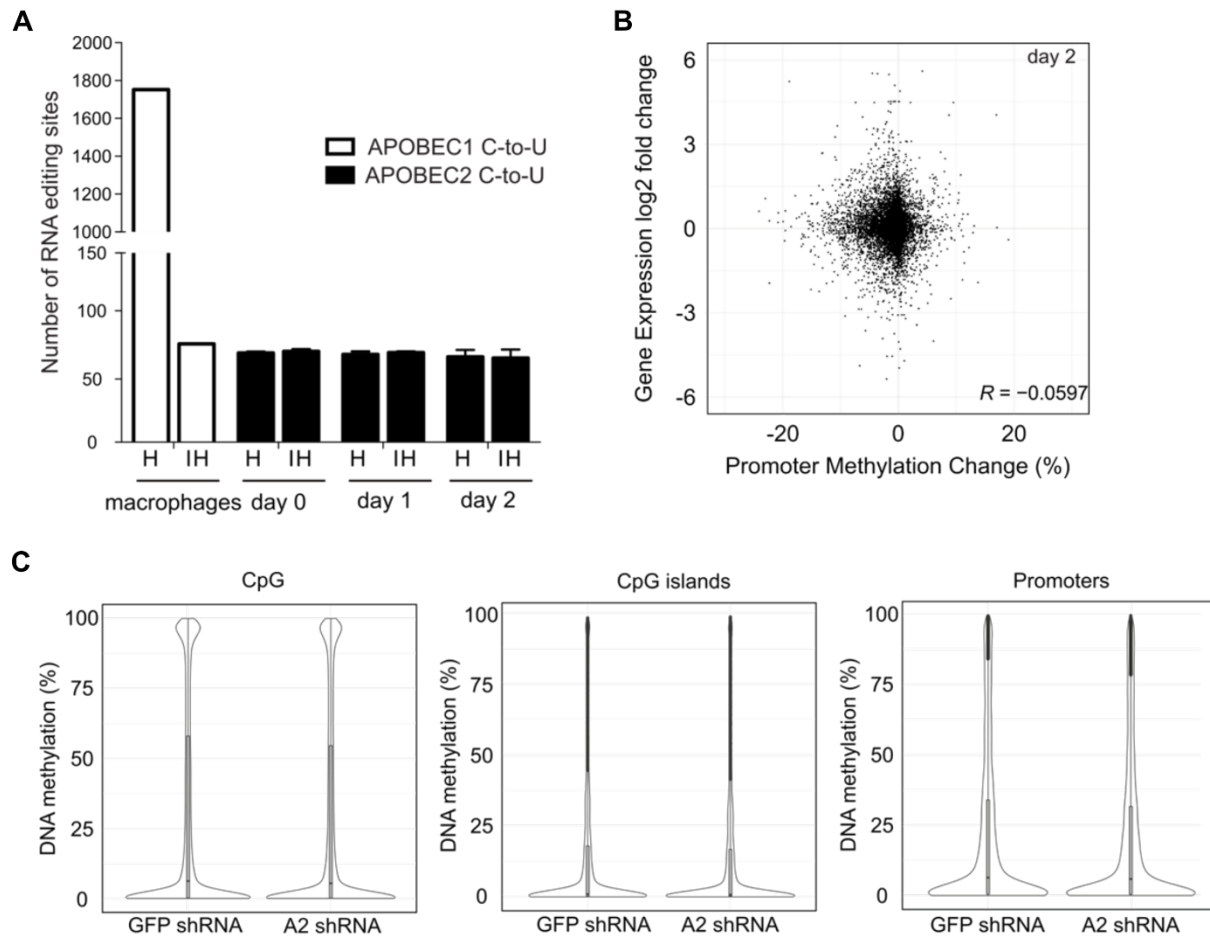
Supplementary Figure 1. C2C12 myoblast differentiation

985
986 (A) Whole cell extracts of mouse wildtype (wt) C2C12 myoblasts and myotubes were
987 analyzed by Western blotting using anti-APOBEC2 antibodies. MyHC and TroponinT were
988 used as markers of late differentiation, alpha-tubulin was used as loading control.

989
990 (B) C2C12 cells were cultured in differentiation medium for 0, 2 and 5 days, fixed, and
991 stained with antibody to MyHC (red). Nuclei were visualized by DAPI staining (blue). Below
992 the quantification of differentiation expressed as fusion index, which is the percentage
993 MyHC-positive myotubes with >2 nuclei. Results are presented as means from quantification
994 of at least 6 images/sample. Error bars indicate SD. Scale bar = 50 μ m.

995
996 (C) Cytoplasmic and nuclear (C and N respectively) were taken from C2C12 cells
997 transduced with vectors to overexpress 3xHA-tagged wildtype APOBEC2 (+ A2-3xHA) and
998 truncated APOBEC2 (+ delA2-3xHA). Western blots were performed with respective lysates
999 using antibodies against HA-tag, APOBEC2, HDAC1, Histone H3, and α Tubulin.

Figure S2



1000
1001

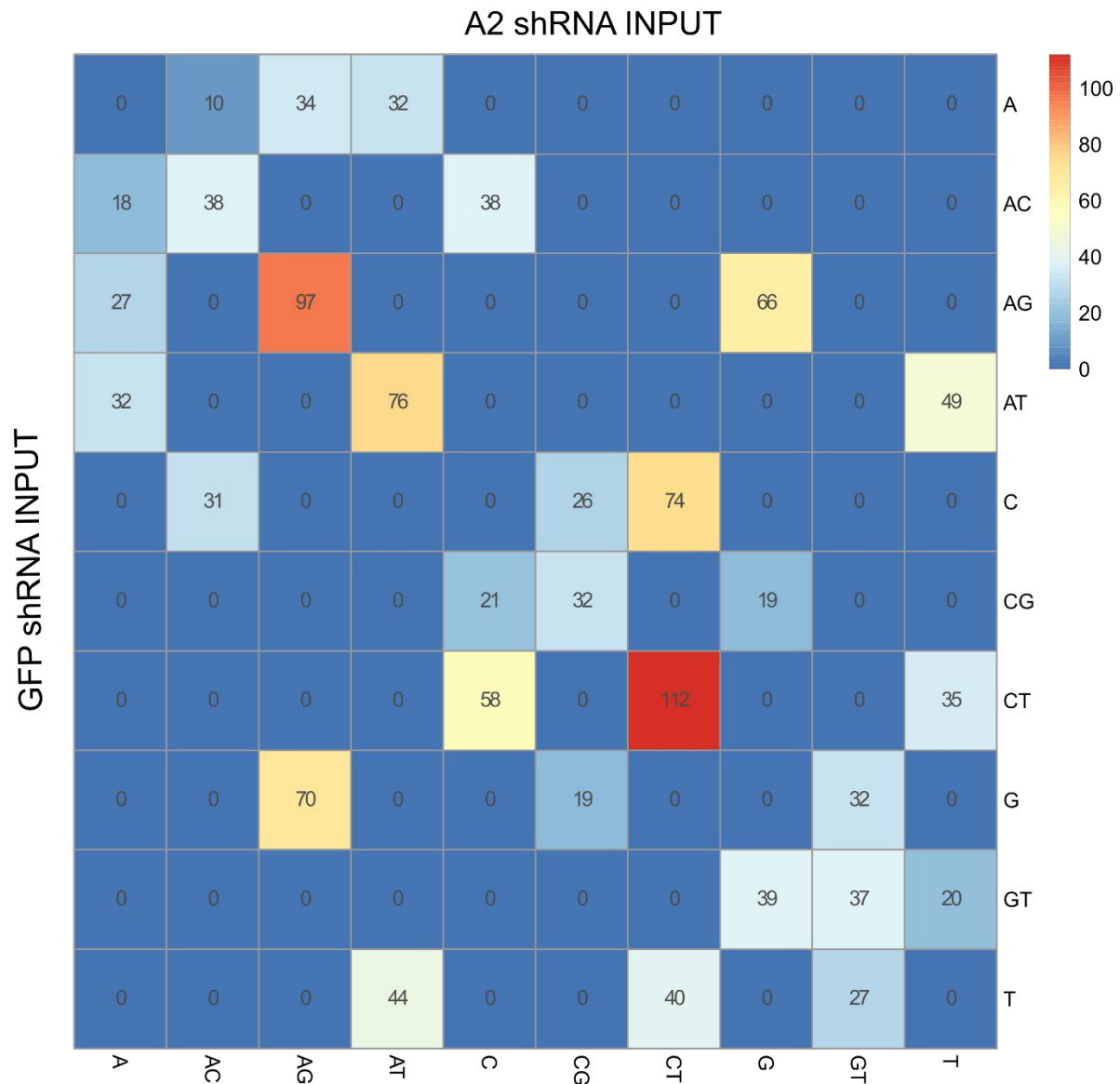
Supplementary Figure 2. mRNA editing and DNA demethylation in C2C12 myoblasts

1002 **(A)** Candidate C-to-U RNA editing sites called from APOBEC2 knockdown samples, control
1003 (GFPsh) at day 0, 1, and 2 in DM in C2C12s and wild-type and APOBEC1^{-/-} macrophages
1004 (positive control). Hits (H) represent candidate editing sites present in control (GFPsh) but
1005 not in APOBEC2 knockdown dataset (in positive control hits are the # of sites in APOBEC1^{-/-}
1006 dataset.) Inverse hits (IH) represent putative edited sites yielded when the inverse
1007 comparison is made, thus edit sites present in the APOBEC2 knockdown dataset but not in
1008 the control (GFPsh) (for the positive control edit sites that are present in APOBEC1^{-/-}
1009 dataset but not in wild-type). Data are represented as means \pm SD using outputs of 3 RNA-
1010 Seq datasets.
1011

1012 **(B)** Methylation changes across all the represented promoters in the ERRBS dataset
1013 compared with the expression changes of the same genes in RNA-Seq dataset. Shown here
1014 are datasets from the day 2 timepoint. R = Pearson's correlation coefficient.
1015
1016

1017 **(C)** Distribution of DNA methylation frequencies in C2C12s as determined by ERRBS for
1018 individual CpGs, CpG islands and promoters. Promoters are defined at \pm 2Kb around the
1019 TSS in Ensemble annotations. CpG islands were taken from the cpGIslandExt track of the
1020 UCSC table browser. Violin plots represent the distribution of DNA methylation frequencies
1021 for each feature. Median and first and third quartiles are shown with the box plots.

Figure S3

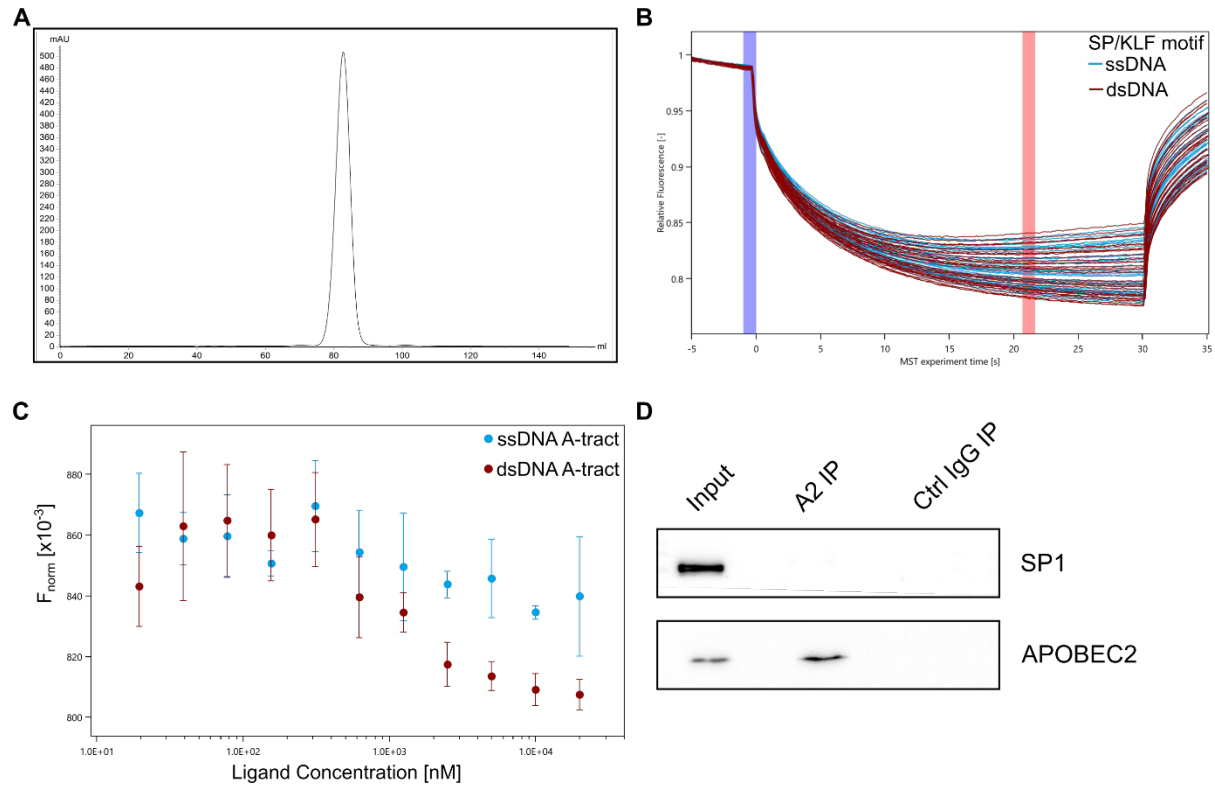


1022
1023
1024
1025
1026

Supplementary Figure 3. DNA Editing in APOBEC2 knockdown versus control (GFP shRNA)

1027 Pairwise heatmap - This is a head-to-head comparison of variant positions between the 2
1028 input sample sets. The symmetry of the heatmap indicates that there is no preference for a
1029 unidirectional base substitution process.

Figure S4



1030
1031

Supplementary Figure 4. Recombinant APOBEC2 electromobility shift assays

1032 **(A)** Size exclusion chromatogram (Superdex 200, GE Healthcare) of recombinant 6x-His-
1033 APOBEC2 produced in High Five/Sf9 (Thermo) insect cells.

1034 **(B)** MST trace for APOBEC2 interaction with ssDNA and dsDNA SP/KLF motifs. Traces
1035 correspond to experiment in Figure 4A. Blue and red highlighted regions represent cold and
1036 hot regions respectively that were used for the standard thermophoresis+ T-jump analysis.

1037 **(C)** MST experiments measuring purified APOBEC2 binding to single-stranded DNA
1038 (ssDNA) or double-stranded (dsDNA) with A-tract motif. Cy5-labeled APOBEC2 was kept
1039 constant (50 nM) while the concentration of non-labeled SP/KLF motif was titrated (1:1
1040 dilution) between 20 nM – 20,000 nM. Normalized fluorescence (F_{norm}) values and graph
1041 were produced with MO.Affinity Analysis v2.1 (NanoTemper Technologies). Values
1042 represent 3 independent measurements with error bars representing the standard deviation.

1043 **(D)** Co-immunoprecipitation (Co-IP) of APOBEC2 with SP1 in C2C12 myoblasts
1044 differentiated to myotubes for 4 days. Nuclear protein lysates (Input) were incubated with
1045 beads conjugated to either APOBEC2 antibody (A2 IP) or IgG isotype control antibody (Ctrl
1046 IgG IP). Proteins were then eluted, ran on an SDS-PAGE gel, and blotted with APOBEC2, or
1047 SP1 antibodies.

1062 GFP-BirA control cells. Nodes in blue indicate proteins that were preferentially labeled by
1063 APOBEC2-BirA compared to AID-BirA in mouse B lymphocytes in a previously published
1064 dataset ⁸². The edges denote the known interactions of these proteins with each as
1065 described in Methods.

1066 **References**

- 1067
- 1068 1. Conticello, S. G. The AID/APOBEC family of nucleic acid mutators. *Genome Biol.* **9**,
 - 1069 229 (2008).
 - 1070 2. Salter, J. D., Bennett, R. P. & Smith, H. C. The APOBEC Protein Family: United by
 - 1071 Structure, Divergent in Function. *Trends Biochem. Sci.* **41**, 578–594 (2016).
 - 1072 3. Cole, D. C. *et al.* Loss of APOBEC1 RNA-editing function in microglia exacerbates
 - 1073 age-related CNS pathophysiology. *Proc. Natl. Acad. Sci.* **114**, 13272–13277 (2017).
 - 1074 4. Rayon-Estrada, V. *et al.* Epitranscriptomic profiling across cell types reveals
 - 1075 associations between APOBEC1-mediated RNA editing, gene expression outcomes,
 - 1076 and cellular function. *Proc. Natl. Acad. Sci.* **114**, 13296–13301 (2017).
 - 1077 5. Harris, R. S. & Dudley, J. P. APOBECs and virus restriction. *Virology* vols 479–480
 - 1078 131–145 (2015).
 - 1079 6. Rai, K. *et al.* DNA Demethylation in Zebrafish Involves the Coupling of a Deaminase,
 - 1080 a Glycosylase, and Gadd45. *Cell* **135**, 1201–1212 (2008).
 - 1081 7. Guo, J. U., Su, Y., Zhong, C., Ming, G. & Song, H. Hydroxylation of 5-Methylcytosine
 - 1082 by TET1 Promotes Active DNA Demethylation in the Adult Brain. *Cell* **145**, 423–434
 - 1083 (2011).
 - 1084 8. Krishnan, A., Iyer, L. M., Holland, S. J., Boehm, T. & Aravind, L. Diversification of
 - 1085 AID/APOBEC-like deaminases in metazoa: multiplicity of clades and widespread roles
 - 1086 in immunity. *Proc. Natl. Acad. Sci. U. S. A.* **115**, E3201–E3210 (2018).
 - 1087 9. Liao, W. *et al.* APOBEC-2, a Cardiac- and Skeletal Muscle-Specific Member of the
 - 1088 Cytidine Deaminase Supergene Family. *Biochem. Biophys. Res. Commun.* **260**, 398–
 - 1089 404 (1999).
 - 1090 10. Sato, Y. *et al.* Deficiency in APOBEC2 Leads to a Shift in Muscle Fiber Type,
 - 1091 Diminished Body Mass, and Myopathy. *J. Biol. Chem.* **285**, 7111–7118 (2010).
 - 1092 11. Etard, C., Roostalu, U. & Strähle, U. Lack of Apobec2-related proteins causes a
 - 1093 dystrophic muscle phenotype in zebrafish embryos. *J. Cell Biol.* **189**, 527–39 (2010).
 - 1094 12. Powell, C., Elsaiedi, F. & Goldman, D. Injury-Dependent Muller Glia and Ganglion Cell
 - 1095 Reprogramming during Tissue Regeneration Requires Apobec2a and Apobec2b. *J.*
 - 1096 *Neurosci.* **32**, 1096–1109 (2012).
 - 1097 13. Vonica, A., Rosa, A., Arduini, B. L. & Brivanlou, A. H. APOBEC2, a selective inhibitor
 - 1098 of TGF β signaling, regulates left-right axis specification during early embryogenesis.
 - 1099 *Dev. Biol.* **350**, 13–23 (2011).
 - 1100 14. Okuyama, S. *et al.* Excessive activity of apolipoprotein B mRNA editing enzyme
 - 1101 catalytic polypeptide 2 (APOBEC2) contributes to liver and lung tumorigenesis. *Int. J.*
 - 1102 *cancer* **130**, 1294–301 (2012).
 - 1103 15. Lohr, J. G. *et al.* Discovery and prioritization of somatic mutations in diffuse large B-
 - 1104 cell lymphoma (DLBCL) by whole-exome sequencing. *Proc. Natl. Acad. Sci. U. S. A.*
 - 1105 **109**, 3879–84 (2012).
 - 1106 16. Powell, C., Cornblath, E. & Goldman, D. Zinc-binding Domain-dependent,
 - 1107 Deaminase-independent Actions of Apolipoprotein B mRNA-editing Enzyme, Catalytic
 - 1108 Polypeptide 2 (Apobec2), Mediate Its Effect on Zebrafish Retina Regeneration. *J. Biol.*
 - 1109 *Chem.* **289**, 28924–28941 (2014).
 - 1110 17. Yaffe, D. & Saxel, O. Serial passaging and differentiation of myogenic cells isolated
 - 1111 from dystrophic mouse muscle. *Nature* **270**, 725–7 (1977).
 - 1112 18. Carrió, E. *et al.* Muscle cell identity requires Pax7-mediated lineage-specific DNA
 - 1113 demethylation. *BMC Biol.* **14**, 30 (2016).
 - 1114 19. Prochnow, C., Bransteitter, R., Klein, M. G., Goodman, M. F. & Chen, X. S. The
 - 1115 APOBEC-2 crystal structure and functional implications for the deaminase AID.
 - 1116 *Nature* **445**, 447–451 (2007).
 - 1117 20. Krzysiak, T. C., Jung, J., Thompson, J., Baker, D. & Gronenborn, A. M. APOBEC2 Is
 - 1118 a Monomer in Solution: Implications for APOBEC3G Models. *Biochemistry* **51**, 2008–
 - 1119 2017 (2012).
 - 1120 21. Watanabe, Y. Conversion of myoblasts to physiologically active neuronal phenotype.

- 1121 *Genes Dev.* **18**, 889–900 (2004).
- 1122 22. Harjanto, D. *et al.* RNA editing generates cellular subsets with diverse sequence
1123 within populations. *Nat. Commun.* **7**, 12145 (2016).
- 1124 23. Laffleur, B. *et al.* AID-induced remodeling of immunoglobulin genes and B cell fate.
1125 *Oncotarget* **5**, 1118–1131 (2014).
- 1126 24. Chan, K. & Gordenin, D. A. Clusters of Multiple Mutations: Incidence and Molecular
1127 Mechanisms. *Annu. Rev. Genet.* **49**, 243–267 (2015).
- 1128 25. Kosugi, S., Hasebe, M., Tomita, M. & Yanagawa, H. Systematic identification of cell
1129 cycle-dependent yeast nucleocytoplasmic shuttling proteins by prediction of
1130 composite motifs. *Proc. Natl. Acad. Sci.* **106**, 10171–10176 (2009).
- 1131 26. Patenaude, A.-M. *et al.* Active nuclear import and cytoplasmic retention of activation-
1132 induced deaminase. *Nat. Struct. Mol. Biol.* **16**, 517–27 (2009).
- 1133 27. Porter, E. G., Connelly, K. E. & Dykhuizen, E. C. Sequential Salt Extractions for the
1134 Analysis of Bulk Chromatin Binding Properties of Chromatin Modifying Complexes. *J.*
1135 *Vis. Exp.* **2017**, (2017).
- 1136 28. Kohli, R. M. *et al.* Local Sequence Targeting in the AID/APOBEC Family Differentially
1137 Impacts Retroviral Restriction and Antibody Diversification. *J. Biol. Chem.* **285**,
1138 40956–40964 (2010).
- 1139 29. Mariani, L., Weinand, K., Vedenko, A., Barrera, L. A. & Bulyk, M. L. Identification of
1140 Human Lineage-Specific Transcriptional Coregulators Enabled by a Glossary of
1141 Binding Modules and Tunable Genomic Backgrounds. *Cell Syst.* **5**, 187-201.e7
1142 (2017).
- 1143 30. Harris, R. S., Petersen-Mahrt, S. K. & Neuberger, M. S. RNA Editing Enzyme
1144 APOBEC1 and Some of Its Homologs Can Act as DNA Mutators. *Mol. Cell* **10**, 1247–
1145 1253 (2002).
- 1146 31. Mikl, M. C. *et al.* Mice Deficient in APOBEC2 and APOBEC3. *Mol. Cell. Biol.* **25**,
1147 7270–7277 (2005).
- 1148 32. Torchy, M. P., Hamiche, A. & Klaholz, B. P. Structure and function insights into the
1149 NuRD chromatin remodeling complex. *Cell. Mol. Life Sci.* **72**, 2491–507 (2015).
- 1150 33. Salter, J. D. & Smith, H. C. Modeling the Embrace of a Mutator: APOBEC Selection of
1151 Nucleic Acid Ligands. *Trends Biochem. Sci.* **43**, 606–622 (2018).
- 1152 34. Vartanian, J., Guétard, D., Henry, M. & Wain-Hobson, S. Evidence for editing of
1153 human papillomavirus DNA by APOBEC3 in benign and precancerous lesions.
1154 *Science* **320**, 230–3 (2008).
- 1155 35. Law, E. K. *et al.* APOBEC3A catalyzes mutation and drives carcinogenesis in vivo. *J.*
1156 *Exp. Med.* **217**, (2020).
- 1157 36. Nabel, C. S. *et al.* AID/APOBEC deaminases disfavor modified cytosines implicated in
1158 DNA demethylation. *Nat. Chem. Biol.* **8**, 751–758 (2012).
- 1159 37. Powell, C., Grant, A. R., Cornblath, E. & Goldman, D. Analysis of DNA methylation
1160 reveals a partial reprogramming of the Muller glia genome during retina regeneration.
1161 *Proc. Natl. Acad. Sci.* **110**, 19814–19819 (2013).
- 1162 38. Gómez-Del Arco, P. *et al.* The Chromatin Remodeling Complex Chd4/NuRD Controls
1163 Striated Muscle Identity and Metabolic Homeostasis. *Cell Metab.* **23**, 881–92 (2016).
- 1164 39. Boija, A. *et al.* Transcription Factors Activate Genes through the Phase-Separation
1165 Capacity of Their Activation Domains. *Cell* **175**, 1842-1855.e16 (2018).
- 1166 40. Lee, Q. Y. *et al.* Pro-neuronal activity of Myod1 due to promiscuous binding to
1167 neuronal genes. *Nat. Cell Biol.* **22**, 401–411 (2020).
- 1168 41. Mall, M. *et al.* Myt1l safeguards neuronal identity by actively repressing many non-
1169 neuronal fates. *Nature* **544**, 245–249 (2017).
- 1170 42. Moffat, J. *et al.* A Lentiviral RNAi Library for Human and Mouse Genes Applied to an
1171 Arrayed Viral High-Content Screen. *Cell* **124**, 1283–1298 (2006).
- 1172 43. Orimo, A. *et al.* Stromal Fibroblasts Present in Invasive Human Breast Carcinomas
1173 Promote Tumor Growth and Angiogenesis through Elevated SDF-1/CXCL12
1174 Secretion. *Cell* **121**, 335–348 (2005).
- 1175 44. Liao, Y., Smyth, G. K. & Shi, W. The Subread aligner: fast, accurate and scalable

- 1176 read mapping by seed-and-vote. *Nucleic Acids Res.* **41**, e108–e108 (2013).
- 1177 45. Lawrence, M., Gentleman, R. & Carey, V. rtracklayer: an R package for interfacing
1178 with genome browsers. *Bioinformatics* **25**, 1841–1842 (2009).
- 1179 46. Lawrence, M. *et al.* Software for Computing and Annotating Genomic Ranges. *PLoS*
1180 *Comput. Biol.* **9**, e1003118 (2013).
- 1181 47. Patro, R., Duggal, G., Love, M. I., Irizarry, R. A. & Kingsford, C. Salmon provides fast
1182 and bias-aware quantification of transcript expression. *Nat. Methods* **14**, 417–419
1183 (2017).
- 1184 48. Soneson, C., Love, M. I. & Robinson, M. D. Differential analyses for RNA-seq:
1185 transcript-level estimates improve gene-level inferences. *F1000Research* **4**, 1521
1186 (2015).
- 1187 49. Love, M. I., Huber, W. & Anders, S. Moderated estimation of fold change and
1188 dispersion for RNA-seq data with DESeq2. *Genome Biol.* **15**, 550 (2014).
- 1189 50. Akalin, A. *et al.* Base-Pair Resolution DNA Methylation Sequencing Reveals
1190 Profoundly Divergent Epigenetic Landscapes in Acute Myeloid Leukemia. *PLoS*
1191 *Genet.* **8**, e1002781 (2012).
- 1192 51. Garrett-Bakelman, F. E. *et al.* Enhanced Reduced Representation Bisulfite
1193 Sequencing for Assessment of DNA Methylation at Base Pair Resolution. *J. Vis. Exp.*
1194 (2015) doi:10.3791/52246.
- 1195 52. Krueger, F. & Andrews, S. R. Bismark: a flexible aligner and methylation caller for
1196 Bisulfite-Seq applications. *Bioinformatics* **27**, 1571–1572 (2011).
- 1197 53. Akalin, A. *et al.* methylKit: a comprehensive R package for the analysis of genome-
1198 wide DNA methylation profiles. *Genome Biol.* **13**, R87 (2012).
- 1199 54. Li, S. *et al.* An optimized algorithm for detecting and annotating regional differential
1200 methylation. *BMC Bioinformatics* **14**, S10 (2013).
- 1201 55. Carroll, T. S., Liang, Z., Salama, R., Stark, R. & de Santiago, I. Impact of artifact
1202 removal on ChIP quality metrics in ChIP-seq and ChIP-exo data. *Front. Genet.* **5**,
1203 (2014).
- 1204 56. Landt, S. G. *et al.* ChIP-seq guidelines and practices of the ENCODE and
1205 modENCODE consortia. *Genome Res.* **22**, 1813–1831 (2012).
- 1206 57. Feng, J., Liu, T. & Zhang, Y. Using MACS to Identify Peaks from ChIP-Seq Data.
1207 *Curr. Protoc. Bioinforma.* **34**, 2.14.1-2.14.14 (2011).
- 1208 58. Zhang, Y. *et al.* Model-based Analysis of ChIP-Seq (MACS). *Genome Biol.* **9**, R137
1209 (2008).
- 1210 59. Yang, Y. *et al.* LEVERAGING BIOLOGICAL REPLICATES TO IMPROVE ANALYSIS
1211 IN CHIP-SEQ EXPERIMENTS. *Comput. Struct. Biotechnol. J.* **9**, e201401002 (2014).
- 1212 60. Yu, G., Wang, L.-G. & He, Q.-Y. ChIPseeker: an R/Bioconductor package for ChIP
1213 peak annotation, comparison and visualization. *Bioinformatics* **31**, 2382–2383 (2015).
- 1214 61. Zhu, L. J. Integrative Analysis of ChIP-Chip and ChIP-Seq Dataset. in *Methods in*
1215 *Molecular Biology* 105–124 (Humana Press, 2013). doi:10.1007/978-1-62703-607-
1216 8_8.
- 1217 62. Zhu, L. J. *et al.* ChIPpeakAnno: a Bioconductor package to annotate ChIP-seq and
1218 ChIP-chip data. *BMC Bioinformatics* **11**, 237 (2010).
- 1219 63. Subramanian, A. *et al.* Gene set enrichment analysis: A knowledge-based approach
1220 for interpreting genome-wide expression profiles. *Proc. Natl. Acad. Sci.* **102**, 15545–
1221 15550 (2005).
- 1222 64. Mi, H. *et al.* Protocol Update for large-scale genome and gene function analysis with
1223 the PANTHER classification system (v.14.0). *Nat. Protoc.* **14**, 703–721 (2019).
- 1224 65. Morita, S., Kojima, T. & Kitamura, T. Plat-E: an efficient and stable system for
1225 transient packaging of retroviruses. *Gene Ther.* **7**, 1063–6 (2000).
- 1226 66. Craig, R. & Beavis, R. C. TANDEM: matching proteins with tandem mass spectra.
1227 *Bioinformatics* **20**, 1466–1467 (2004).
- 1228 67. Shteynberg, D. *et al.* iProphet: Multi-level Integrative Analysis of Shotgun Proteomic
1229 Data Improves Peptide and Protein Identification Rates and Error Estimates. *Mol.*
1230 *Cell. Proteomics* **10**, M111.007690 (2011).

- 1231 68. Liu, G. *et al.* ProHits: integrated software for mass spectrometry–based interaction
1232 proteomics. *Nat. Biotechnol.* **28**, 1015–1017 (2010).
- 1233 69. Keller, A., Nesvizhskii, A. I., Kolker, E. & Aebersold, R. Empirical Statistical Model To
1234 Estimate the Accuracy of Peptide Identifications Made by {MS}{MS} and Database
1235 Search. *Anal. Chem.* **74**, 5383–5392 (2002).
- 1236 70. Nesvizhskii, A. I., Keller, A., Kolker, E. & Aebersold, R. A Statistical Model for
1237 Identifying Proteins by Tandem Mass Spectrometry. *Anal. Chem.* **75**, 4646–4658
1238 (2003).
- 1239 71. Teo, G. *et al.* SAINTexpress: Improvements and additional features in Significance
1240 Analysis of INTeractome software. *J. Proteomics* **100**, 37–43 (2014).
- 1241 72. Anders, S. & Huber, W. Differential expression analysis for sequence count data.
1242 *Genome Biol.* **11**, R106 (2010).
- 1243 73. Shannon, P. Cytoscape: A Software Environment for Integrated Models of
1244 Biomolecular Interaction Networks. *Genome Res.* **13**, 2498–2504 (2003).
- 1245 74. Chatr-Aryamontri, A. *et al.* The BioGRID interaction database: 2017 update. *Nucleic
1246 Acids Res.* **45**, D369–D379 (2017).
- 1247 75. Orchard, S. *et al.* The MIntAct project—IntAct as a common curation platform for 11
1248 molecular interaction databases. *Nucleic Acids Res.* **42**, D358–D363 (2014).
- 1249 76. Morris, J. H. *et al.* clusterMaker: a multi-algorithm clustering plugin for Cytoscape.
1250 *BMC Bioinformatics* **12**, 436 (2011).
- 1251 77. Huntley, R. P. *et al.* The GOA database: Gene Ontology annotation updates for 2015.
1252 *Nucleic Acids Res.* **43**, D1057–D1063 (2015).
- 1253 78. Giurgiu, M. *et al.* CORUM: the comprehensive resource of mammalian protein
1254 complexes-2019. *Nucleic Acids Res.* **47**, D559–D563 (2019).
- 1255 79. Merico, D., Isserlin, R., Stueker, O., Emili, A. & Bader, G. D. Enrichment map: a
1256 network-based method for gene-set enrichment visualization and interpretation. *PLoS
1257 One* **5**, e13984 (2010).
- 1258 80. Raudvere, U. *et al.* g:Profiler: a web server for functional enrichment analysis and
1259 conversions of gene lists (2019 update). *Nucleic Acids Res.* **47**, W191–W198 (2019).
- 1260 81. Mi, H., Muruganujan, A., Ebert, D., Huang, X. & Thomas, P. D. PANTHER version 14:
1261 more genomes, a new PANTHER GO-slim and improvements in enrichment analysis
1262 tools. *Nucleic Acids Res.* **47**, D419–D426 (2019).
- 1263 82. Methot, S. P. *et al.* A licensing step links AID to transcription elongation for
1264 mutagenesis in B cells. *Nat. Commun.* **9**, 1248 (2018).
- 1265